

RESEARCH ARTICLE

Expansion microscopy using a single anchor molecule for high-yield multiplexed imaging of proteins and RNAs

Yi Cui^{1,2}[✉], Gaojie Yang^{1,2}[✉], Daniel R. Goodwin^{1,2}, Ciara H. O'Flanagan³, Anubhav Sinha^{1,2,4}[✉], Chi Zhang^{1,2}, Kristina E. Kitko^{1,2}[✉], Tay Won Shin^{1,2}[✉], Demian Park^{1,2}, Samuel Aparicio^{3,5}, CRUK IMAXT Grand Challenge Consortium¹, Edward S. Boyden^{1,2,6,7,8,9}^{*}

1 McGovern Institute, Massachusetts Institute of Technology (MIT), Cambridge, Massachusetts, United States of America, **2** Media Arts & Sciences, MIT, Cambridge, Massachusetts, United States of America, **3** Department of Molecular Oncology, BC Cancer, Vancouver, British Columbia, Canada, **4** Harvard-MIT Program in Health Sciences and Technology, MIT, Cambridge, Massachusetts, United States of America, **5** Department of Pathology and Laboratory Medicine, University of British Columbia, Vancouver, British Columbia, Canada, **6** Department of Biological Engineering, MIT, Cambridge, Massachusetts, United States of America, **7** Department of Brain and Cognitive Sciences, MIT, Cambridge, Massachusetts, United States of America, **8** Koch Institute for Cancer Research, MIT, Cambridge, Massachusetts, United States of America, **9** Howard Hughes Medical Institute, MIT, Cambridge, Massachusetts, United States of America

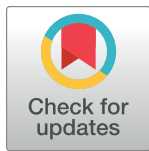
 These authors contributed equally to this work.

[✉] Current address: NanoString Technologies, Inc., Seattle, Washington, United States of America

[✉] Current address: Eli Lilly and Company, San Francisco, California, United States of America

[¶] List of the IMAXT Consortium investigators is provided in the Acknowledgments.

* edboyden@mit.edu


 OPEN ACCESS

Citation: Cui Y, Yang G, Goodwin DR, O'Flanagan CH, Sinha A, Zhang C, et al. (2023) Expansion microscopy using a single anchor molecule for high-yield multiplexed imaging of proteins and RNAs. PLoS ONE 18(9): e0291506. <https://doi.org/10.1371/journal.pone.0291506>

Editor: Bing Xu, Brandeis University, UNITED STATES

Received: May 28, 2023

Accepted: August 30, 2023

Published: September 20, 2023

Copyright: © 2023 Cui et al. This is an open access article distributed under the terms of the [Creative Commons Attribution License](https://creativecommons.org/licenses/by/4.0/), which permits unrestricted use, distribution, and reproduction in any medium, provided the original author and source are credited.

Data Availability Statement: All relevant data are within the paper and its [Supporting information files](#).

Funding: E.S.B. acknowledges for funding, Lisa Yang, John Doerr, Open Philanthropy, Tom Stocky, NIH 1R01EB024261, Kathleen Octavio, Lore McGovern, NIH 1R01AG070831, HHMI, NIH 1R01MH123403, ERC Synergy Grant agreement No 835102, NIH R01MH124606, NIH R37MH080046, NIH U24NS109113, NIH 1U19MH114821, and the Cancer Research UK

Abstract

Expansion microscopy (ExM), by physically enlarging specimens in an isotropic fashion, enables nanoimaging on standard light microscopes. Key to existing ExM protocols is the equipping of different kinds of molecules, with different kinds of anchoring moieties, so they can all be pulled apart from each other by polymer swelling. Here we present a multifunctional anchor, an acrylate epoxide, that enables proteins and RNAs to be equipped with anchors in a single experimental step. This reagent simplifies ExM protocols and reduces cost (by 2–10-fold for a typical multiplexed ExM experiment) compared to previous strategies for equipping RNAs with anchors. We show that this united ExM (uniExM) protocol can be used to preserve and visualize RNA transcripts, proteins in biologically relevant ultrastructures, and sets of RNA transcripts in patient-derived xenograft (PDX) cancer tissues and may support the visualization of other kinds of biomolecular species as well. uniExM may find many uses in the simple, multimodal nanoscale analysis of cells and tissues.

Introduction

Nanoscale imaging enables the analysis of biological systems, such as cells and tissues, at the fundamental length scales of biomolecules and biomolecular interactions, but classically has required expensive equipment and advanced skillsets to perform, *e.g.*, via super-resolution microscopy [1]. Recently, expansion microscopy (ExM), which physically magnifies biological

Grand Challenge grant C31893/A25050. The funders had no role in study design, data collection and analysis, decision to publish, or preparation of the manuscript.

Competing interests: Y.C., G.Y. and E.S.B. have filed for provisional patent protection on the design, steps and applications of uniExM through MIT Technology Licensing Office (U.S. Appl. No. 63/326,346). E.S.B. is a cofounder of the company Expansion Technologies to help with commercialization of ExM related techniques. This does not alter our adherence to PLoS ONE policies on sharing data and materials.

specimens through a chemical process, thus enabling nanoimaging on conventional microscopes [2–4]. has become popular, with hundreds of experimental papers and preprints exploring a diversity of biological systems with nanoscale precision [5]. ExM protocols comprise several typical steps: first, one or more molecular anchors are introduced to covalently bond with target biomolecules, or labels bound to those molecules (*e.g.*, endogenous proteins or nucleic acids, or fluorescent probes bound to them); second, acrylate monomers are infused and then polymerized into a swellable polyacrylate hydrogel network that also binds to the anchors; third, the resultant specimen-hydrogel composite is subjected to denaturation or enzymatic digestion to free up inter/intra-molecular connections (*e.g.*, fixative crosslinks), or even to dissolve molecules no longer needed for visualization; finally, the sample is isotropically expanded (typically $\sim 4.5\times$ in the most commonly used protocols [6]) upon dialysis with an excess of water (Fig 1A). ExM has been successfully demonstrated in a wide range of sample types and given rise to a number of variants tackling specialized purposes, *e.g.*, higher magnification factors, adaptation to human tissues, decrowding of molecules for better access by labels, and multiplexed molecular imaging [7–26], to name a few, which have been used to study a diversity of topics in virology, molecular biology, neuroscience, cancer biology, and other fields within biology and medicine.

Although most papers performing ExM investigate a single kind of biomolecule, *e.g.*, proteins, an increasing number of studies are seeking to investigate multiple kinds of molecule, *e.g.*, both proteins and RNAs [4, 21, 27, 28]. The recently published Magnify protocol yielded images of RNA being visualized in cultured cells, but the RNA yield was not measured, nor compared to earlier methods in terms of quantitative performance; furthermore, dual RNA and protein visualization in the same sample was not performed [29]. Except for this protocol, all other protocols for examining both proteins and RNAs to date have required different anchors—proteins have been bound by molecules that connect amines to a vinyl group (*e.g.*, through the molecule AcX) [3, 7, 8], whereas RNAs have been bound by molecules that alkylate guanines (*e.g.*, through the molecule LabelX) [4, 27] (schematics in S1 Fig in S1 File). The RNA anchors are made by mixing off-the-shelf chemicals overnight; the RNA anchors are sometimes applied to the specimen in a separate step from the protein anchors, adding time and complexity to the procedure. The need for in-house synthesis adds a potential uncertainty to the overall process, since individuals may not conduct the reaction under identical conditions in all groups, resulting in non-controlled final yield. The cost of the RNA-binding reagents is also high—LabelX and MelphaX (AcX reacted with Label-IT amine and Melphalan, respectively), the two molecules used to date, cost \$7,500 and \$70 per mg, respectively, as of late 2022, resulting in overall experimental costs of \$180 and \$40, respectively, for a typical sample (*e.g.*, a 50–100 μm thick full-width mouse brain slice. Here we introduce, and validate, an epoxide-based anchoring strategy that enables proteins and RNAs to be anchored to the hydrogel in a single step, in an inexpensive fashion, without requiring any end-user synthesis. We demonstrated the versatility of this united ExM (uniExM) protocol in the analysis of proteins and RNAs, as well as in multiplexed settings such as that of expansion sequencing (ExSeq) [21], suggesting the utility of epoxide anchoring in a diversity of high-resolution spatial biology studies.

Materials and methods

Cell culture and mouse brain tissues

HeLa cells were cultured in DMEM medium supplemented with 10% FBS and 1% penicillin-streptomycin antibiotics. Once the cells reached 70–80% confluence, they were fixed with either 4% paraformaldehyde (PFA) or 3% PFA/0.1% glutaraldehyde (GA, for better

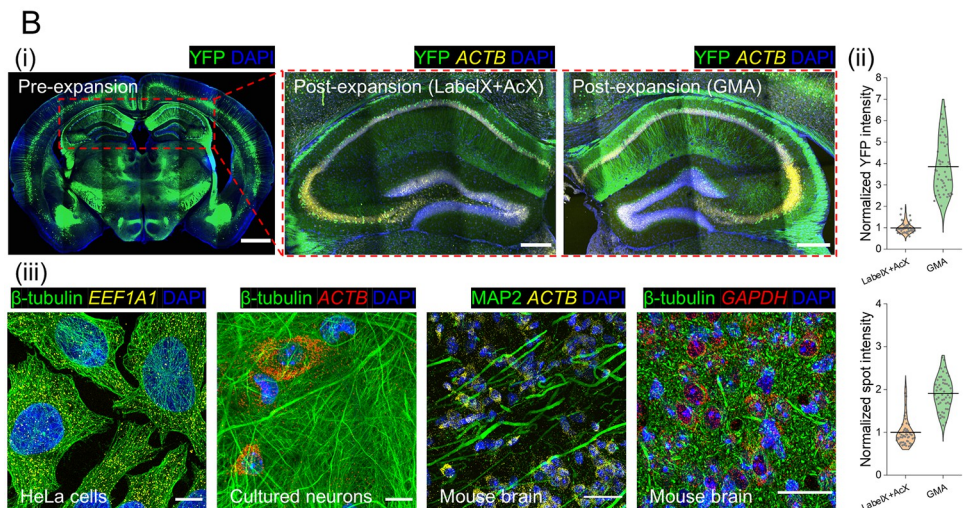
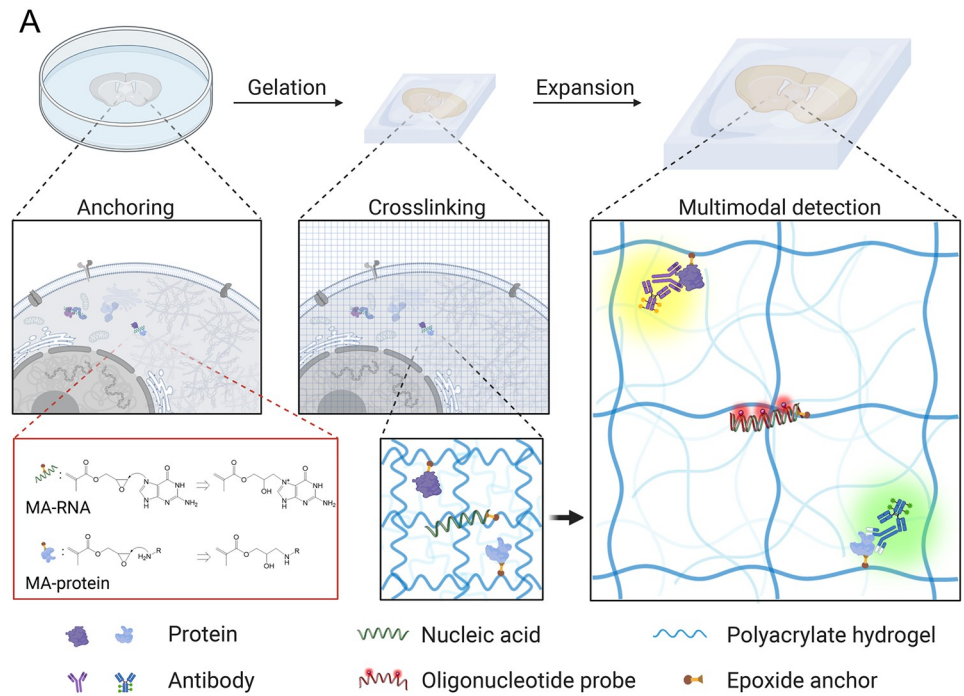


Fig 1. An epoxide anchor enables expansion of proteins and RNAs away from each other. (A) In a standard ExM experiment, target biomolecules (e.g., proteins and nucleic acids, or labels attached to them) in a biological specimen are covalently bound to anchoring molecules bearing vinyl groups (here, an epoxide such as glycidyl methacrylate (GMA), turning biomolecules to methacrylate (MA) forms, e.g., MA-RNA and MA-protein) that can be crosslinked to a swellable polyacrylate hydrogel synthesized throughout the specimen (“Gelation”). After tissue softening with denaturation and/or proteolysis, the sample can be isotropically expanded upon dialysis with low osmolarity solutions (e.g., distilled water), during which the anchored biomolecules are pulled apart (“Expansion”). Target-specific detection can be performed (e.g., antibody staining for proteins and oligonucleotide probe hybridization for RNAs) to realize nanoimaging on conventional microscopes. (B) Using the epoxide anchor GMA, simultaneous detection of nucleic acids and proteins was demonstrated across different sample types. In panel (i), a 50 μm thick coronal section of mouse brain tissue expressing Thy1-YFP was cut in half, one part anchored with 0.01% (w/v) LabelX plus 0.005% (w/v) AcX and the other with 0.1% (w/v) GMA. The samples were then subjected to gelation and proK based digestion. HCR-FISH targeting *ACTB* mRNAs was performed post-expansion and the FISH signals were quantified together with the retained YFP signals. Scale bars (in pre-expansion units): 1000 μm (whole brain); 250 μm (zoomed-in hippocampal view). Linear expansion factor: 4.1. In panel (ii), mean intensities for YFP within cells and HCR-FISH spots in each image were quantified and compared between the LabelX/AcX and GMA processed tissues (data distribution shown in violin plots, with raw data points presented, and mean values highlighted with solid lines; n = 50

images from 3 different slices, 2 mouse brains; two-sample *t*-test was performed with $p < 10^{-20}$ for both YFP and HCR-FISH signals). In panel (iii), multimodal detection of proteins and RNAs with uniExM was demonstrated. Antibody staining for proteins was performed pre-expansion and the samples were anchored with 0.04% (w/v) GMA (for HeLa cells and cultured neurons) or 0.1% (w/v) GMA (for mouse brain slices). After gelation and expansion, HCR-FISH targeting specific RNA targets was performed post-expansion. In the figure captions, capitalized italic fonts represent the RNA target names (*ACTB*, *EEF1A1*, *GAPDH*). The colors in each image correspond to the following fluorescent dyes: blue—DAPI; green—Alexa488; yellow—Alexa546; red—Alexa647. Scale bars (in pre-expansion units): 20 μm . Linear expansion factors: 4.4 for HeLa cells and cultured neurons, 4.1 for mouse brain tissues (prior to re-embedding). All images are shown as maximum z-projection of image stacks (10–15 μm z-depth for cultured HeLa cells and neurons; 50 μm for mouse brain tissues).

<https://doi.org/10.1371/journal.pone.0291506.g001>

preservation of intracellular fine structures including β -tubulin and β II-spectrin in Figs 1B iii, 2A and 3, S7, S13B Figs in S1 File), followed by residual aldehyde quenching with 0.1% sodium borohydride and 100 mM glycine. For RNA detection (ExFISH and ExSeq), samples were permeabilized and stored with 70% ethanol at 4°C overnight or up to 4 weeks.

All procedures involving animals were in accordance with the US National Institutes of Health Guide for the Care and Use of Laboratory Animals and approved by the Massachusetts Institute of Technology Committee on Animal Care. Primary neurons were dissected from brains isolated from euthanized newborn Swiss Webster mice and about 1,000 hippocampal neurons were seeded onto a 12 mm #1.5 coverslip. The neurons were cultured with MEM medium containing 33 mM glucose, 0.01% transferrin, 10 mM HEPES, 2 mM Glutagro, 0.13% insulin, 2% B27 supplement, and 7.5% heat-inactivated FBS at 37°C in a humid incubator supplemented with 5% CO₂ for 2 weeks and then fixed for subsequent uses.

For mouse brain tissues, three seven-week-old mice were terminally anesthetized with isoflurane, followed by transcardial perfusion with PBS and ice cold 4% PFA. Then the brain was dissected out and placed in 4% PFA for 12–16 hours. 50 μm slices were prepared on a vibratome (Leica VT1000s) and then stored at 4°C in PBS (for lipid co-detection in S13 Fig in S1 File) or 70% ethanol until use. Animal health and behavior were fully assessed twice a week before euthanasia.

Patient-derived xenografts (PDX)

Patient tumor sample xeno-transplanted was acquired in 2011 according to procedures approved by the Ethics Committees at the University of British Columbia. Sample from breast cancer patients undergoing diagnostic biopsy or surgery were collected under protocol H06-00289 (BCCA-TTR-BREAST). Written informed consent was obtained and documented by UBC BC Cancer Research Ethics Board electronically and or in writing. All data were fully anonymized. Tumor fragments were finely chopped and mechanically disaggregated for one minute using a Stomacher 80 Biomaster (Seward Limited, Worthing UK) in 1 mL cold DMEM/F-12 with Glucose, L-Glutamine and HEPES (Lonza 12-719F). 200 μL of medium containing cells/organoids from the suspension was used for transplantation per mouse. Tumors were transplanted in mice as previously described in accordance with SOP BCCRC 009 [30] in 2020. Female NOD/SCID/IL2R γ $-/-$ (NSG) and NOD/Rag1 $-/-$ IL2R γ $-/-$ (NRG) mice were bred and housed at the Animal Resource Centre at the British Columbia (BC) Cancer Research Centre. Disaggregated cells and organoids were resuspended in 150–200 μL of a 1:1 v/v mixture of cold DMEM/F12: Matrigel (BD Biosciences, San Jose, CA, USA). 8–12-week-old mice were anesthetized with isoflurane and the suspension was transplanted under the skin on the left flank using a 1 mL syringe and 21-gauge needle. One xenograft-bearing mouse was used; it was euthanized for tissue collection when the size of tumor approached 1 mL in volume. The animal care committee and animal welfare and ethical review committee,

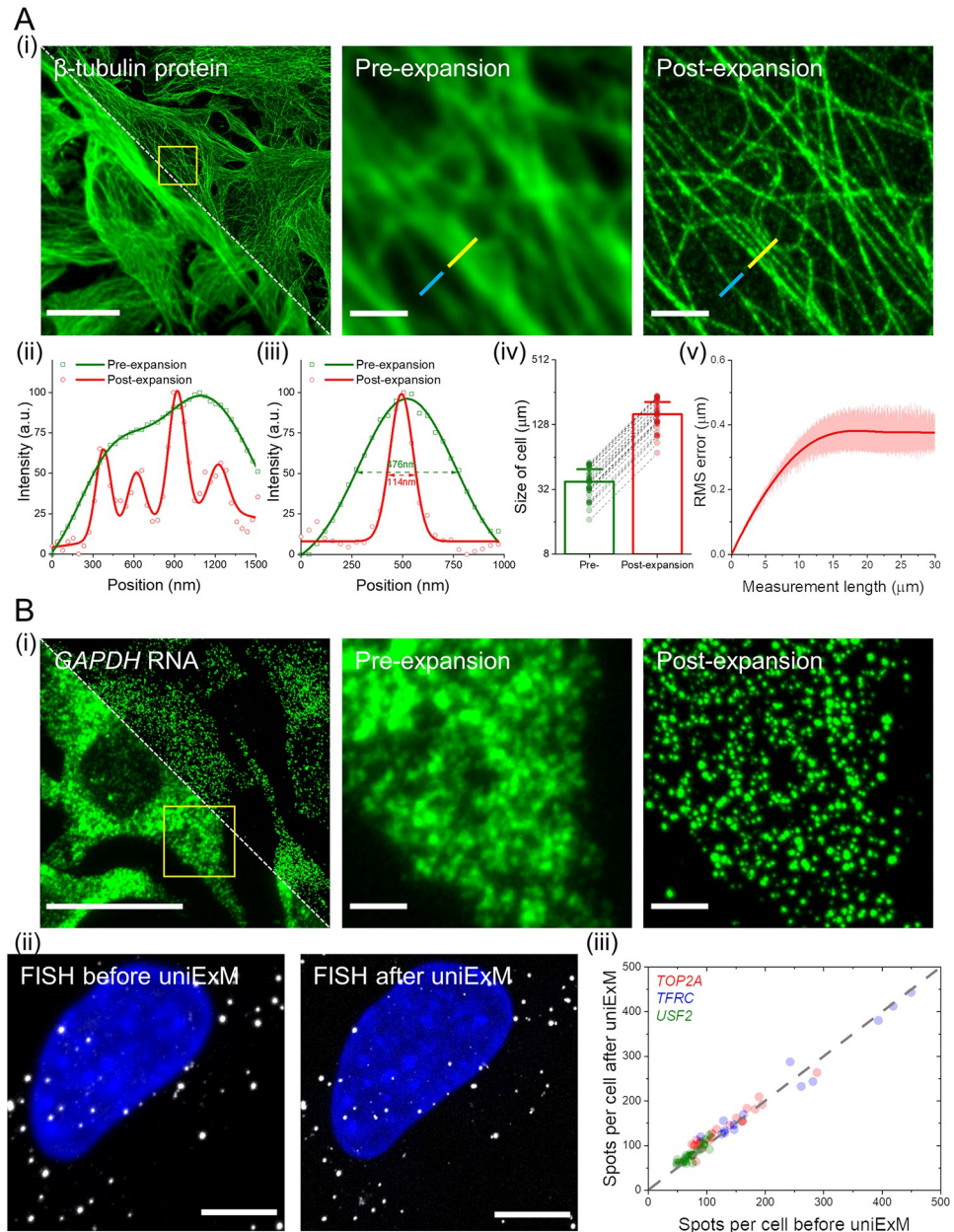


Fig 2. Characterization of GMA-based uniExM for protein and RNA retention. (A) uniExM improves imaging resolution and achieves homogenous expansion. (i) Representative images of HeLa cells stained with β -tubulin antibody (pre-expansion staining) are shown. Upon expansion, resolution improvement, expansion factor and distortion were evaluated. Left image: pre-expansion (lower left half) and post-expansion (upper right half) fields of view of the same specimen, where the white diagonal dashed line delineates the boundary between the two images. Middle and right images: zoomed-in view of the region highlighted by the yellow square in the left image. Scale bars (in pre-expansion units): 20 μm (left image), 2 μm (middle and right images). Panels (ii) and (iii) plot the cross-section intensity profiles along the yellow and blue lines, respectively, in the zoomed-in images of panel (i). The raw intensity values (shapes) were fitted with multi-peak Gaussian functions (solid lines). The values presented in panel (iii) are FWHM (full width at half maximum) of the fitted Gaussian functions. In panel (iv), long axes of the same cell were measured before and after expansion to calculate the expansion factor. The linear expansion factor was determined to be 4.2 in this demonstration ($n = 30$ cells from 2 different batches of culture; mean + standard deviation was presented in bar chart with raw measurements shown as individual points). In panel (v), RMS length measurement error was quantified by benchmarking post-expansion confocal images against pre-expansion super-resolution SoRa images of microtubule staining in HeLa cells (red line, mean value; shaded area, standard deviation; $n = 5$ samples). (B) uniExM for RNA detection and quantification. (i) GMA-based expansion helps de-crowd densely packed mRNAs and better

resolve single transcripts of the highly expressed *GAPDH* gene in HeLa cells. Left image: pre-expansion (lower left half) and post-expansion (upper right half) images of the same specimen, where the white diagonal dashed line delineates the boundary between these two images. Middle and right images: zoomed-in view of the region highlighted by the yellow square in the left image. Scale bars (in pre-expansion units): 20 μm (left image), 2 μm (middle and right images). (ii) GMA-based uniExM effectively preserves RNA information during the expansion process. HCR-FISH targeting specific genes was performed before and after expansion. Left image: a representative image of HCR-FISH for the *USF2* gene in HeLa cells. Number of transcripts per cell was counted, and then FISH probes were stripped off with concentrated formamide and heating. Right image: The same sample was subjected to uniExM, after which HCR-FISH targeting the same gene was performed and quantified. Scale bars (in pre-expansion units): 5 μm . (iii) Three genes—*TOP2A*, *TFRC* and *USF2* (with the expression level ranging from ~50 to ~500 transcripts per cell)—were chosen to evaluate the RNA anchoring efficiency by GMA in uniExM. Spots/transcripts per cell counted before and after GMA anchoring were fit by linear regression, with an R-squared value of 0.9736, indicating nearly 100% RNA retention (each point in the scatter plot represents one measurement from a single cell; $n = 60$ cells collected from 3 culture batches).

<https://doi.org/10.1371/journal.pone.0291506.g002>

the University of British Columbia (UBC), approved all experimental procedures. Animal health and behavior were monitored daily, and fully assessed twice a week before euthanasia.

Anchoring, gelation, homogenization and expansion

Fixed cells and tissue slices were first pre-incubated with 100 mM sodium bicarbonate (pH = 8.5, DNase/RNase-free) twice for 15 min each, and incubated in GMA in 100 mM sodium bicarbonate for 3 h at room temperature or 37°C, dependent on target and sample types (detailed anchoring conditions are provided in S4 Table in S1 File). Of particular note, the solubility of GMA is about 3% in most aqueous solutions and so the anchoring buffer has to be vigorously vortexed after addition of GMA. According to the safety data sheet of GMA, handling of undiluted GMA needs to be done in a fume hood with sufficient ventilation. For experiments using cultured cells, 0.04% (w/v) GMA was used for anchoring, while 0.1% (w/v) GMA was used for tissue samples. For ease of use, the GMA reaction can be left at room temperature overnight without adverse effects. After the anchoring reaction, samples were washed with sterile PBS or DPBS three times (for samples using >0.2% GMA in the concentration optimization experiments of S5 Fig in S1 File, they were washed with 70% ethanol to remove unreacted GMA before washing with DPBS). Then, standard ExM steps including gelation, digestion and expansion were conducted.

Briefly, for gelation, the monomer solution—StockX—was prepared as developed in unpublished protocols [6]: 8.6% (w/v) sodium acrylate (SA), 2.5% (w/v) acrylamide (AA), 0.15% (w/v) N,N'-methylenebisacrylamide (Bis), 2 M sodium chloride (NaCl), 1× PBS. Then the gelation solution was prepared by mixing StockX with 0.5% (w/v) 4-Hydroxy-TEMPO (4-HT) stock solution (required for tissue samples), 10% (w/v) N,N,N',N'-Tetramethylethylenediamine (TEMED) stock solution, and 10% (w/v) ammonium persulfate (APS) stock solution at 47:1:1:1 ratio on a 4°C cold block, and diffused into the sample at 4°C for 30 min. #0 coverslips were used as spacers between two slides to make a gelling chamber, to cast the gel with thickness around 100 μm . Next, the gelling chamber containing the tissue with infiltrated gelation solution was transferred to a sealed Tupperware for free-radical initiated polymerization at 37°C (a detailed ExM manual can be found here [31]). For the modified 7× expansion protocol, the following monomer solution was used (adapted from the TREx protocol [26]): 17.5% SA, 5% AA, 0.015% Bis, 2 M NaCl, 1× PBS, and mixed with 10% TEMED and APS at 198:1:1 ratio. To reduce the gel attachment to glass surfaces, the glassware can be briefly rinsed with Sigmacote reagent before use.

After 2 hours, the gelled sample was removed from the chamber, trimmed to the proper size, where only the areas of interest were kept, and then immersed in digestion buffer. Different sample homogenization methods were applied as specified below.

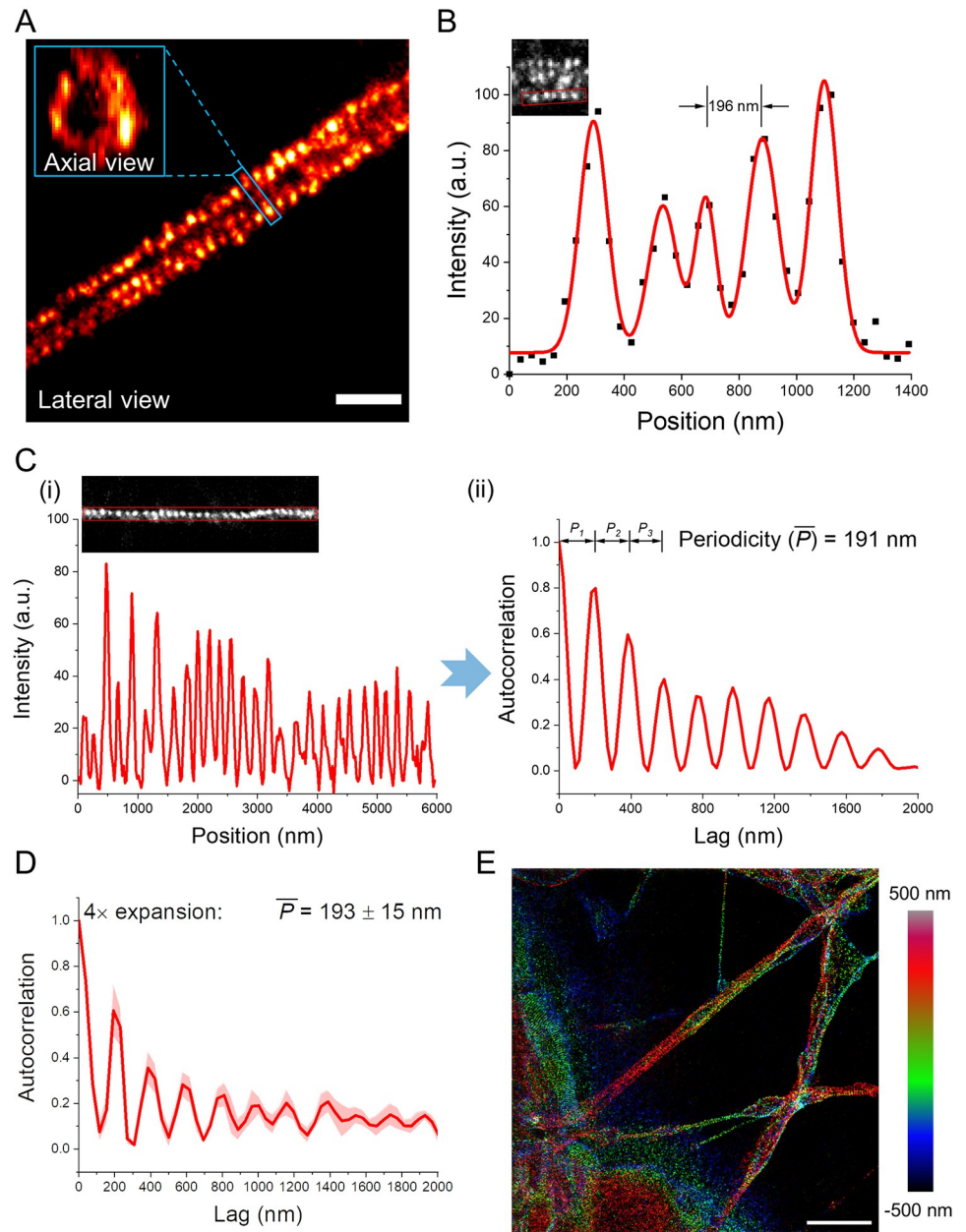


Fig 3. Preservation of protein ultrastructural organization by GMA in uniExM. (A) Antibody staining against β II-spectrin in mouse hippocampal neurons was performed with 4 \times expansion (linear expansion factor ~ 4.2). One segment of axon showing periodic, punctate signals is presented. In the zoomed-in inset, the axial view of β II-spectrin is shown, displaying a ring structure. Scale bar (in pre-expansion units): 1 μ m. (B) The intensity profile of β II-spectrin clusters along an axon segment (within the red rectangle of the inset image) was plotted and fitted with multi-peak Gaussian functions (black squares: raw data points; red line: fitting function). A consistent distance around 190 nm between two adjacent peaks was noted. (C) Antibody staining against β II-spectrin in mouse hippocampal neurons was performed with a 7 \times expansion protocol modified from the TReX protocol (linear expansion factor ~ 7.3). (i) The intensity profile of over 10 β II-spectrin clusters along an axon segment (within the red rectangle of the inset image) was plotted. (ii) Autocorrelation analysis was performed to calculate the periodicity of β II-spectrin clusters across space (*i.e.*, the similarity between signals as a function of the spatial position lag between them). Based on each fitted autocorrelation function, the first three inter-peak distance values (denoted as P_1 , P_2 and P_3) were extracted to calculate the mean periodicity \bar{P} . (D) Mean autocorrelation function of periodicity analysis using 4 \times expansion and pre-expansion antibody staining. (Solid lines, mean; shaded areas, standard error of mean. $n = 40$ measurements from 2 culture batches). (E) Post-expansion antibody staining revealed the same periodic distribution pattern of β II-spectrin under 4 \times expansion. Scale bar (in pre-expansion units): 5 μ m. The color code of the image represents z-axis information.

<https://doi.org/10.1371/journal.pone.0291506.g003>

For experiments in Figs 1–3, S4–S6, S10, S11A, S11B Figs in [S1 File](#), the standard proteinase K (proK) based digestion method was performed with the buffer containing 8 U/ml proK, 0.5% (w/v) Triton X-100, 1 mM EDTA, 50 mM Tris-HCl buffer (pH = 8), and 2 M NaCl. The gelled samples were digested at 37°C overnight.

For the comparison experiments of LabelX/AcX and epoxides in preservation of proteins under high heat treatments (S8 Fig in [S1 File](#)), two homogenization methods were tested. In the heat-based SDS denaturation, gels were incubated with the denaturation buffer containing 200 mM SDS, 200 mM NaCl, and 50 mM Tris base (pH = 9) at 95°C for 1 hour, followed by incubation at 37°C overnight and washing with 0.2% TritonX-100 in fresh PBS to remove residual SDS before expansion. In the proK based rapid digestion, gels were digested with 8 U/ml proK, 0.8 M guanidine hydrochloride, 0.5% (w/v) Triton X-100, 1 mM EDTA, 50 mM Tris-HCl buffer (pH = 8), and 2 M NaCl at 60°C for 2 hours, followed by incubation with fresh digestion buffer at 37°C overnight before expansion.

For post-expansion antibody staining and experiments involving WGA staining (S3, S11C, S12C, S13 Figs in [S1 File](#)), gelled samples were digested with 50 µg/mL (for cells) or 100 µg/mL (for tissues) endoproteinase LysC in 1 mM EDTA, 50 mM Tris-HCl (pH = 8) and 0.1 M NaCl at 37°C overnight (for cells) or 2–3 days (for tissues). For post-expansion antibody staining targeting Thy1-YFP in mouse brain tissues (S3 Fig in [S1 File](#)), the heat-based SDS denaturation was applied.

After homogenization, the gelled samples were rinsed 3 times with fresh PBS, followed by expansion with ion-free, ultrapure water (3 × 15 min for cells, 3 × 30 min for tissues). To expand LysC-digested tissues, serial incubation with decreasing PBS (1×, 0.5×, 0.1×, 30 min each) or NaCl solutions (1M, 0.5M, 0.1M, 30 min each) was conducted before expansion with water.

Pre-expansion antibody staining

To assess the potential sample distortion during the GMA-based uniExM procedure and the improvement on imaging resolution, pre-expansion antibody staining was performed. Primary antibodies against β -tubulin, MAP2, neurofilament, GFP, and β II-spectrin were used to stain predetermined structures in different samples. In brief, samples were fixed with 3% PFA/0.1% GA (for microtubule and spectrin preservation) or 4% PFA, followed by processing with 0.1% sodium borohydride and 100 mM glycine to quench unreacted fixative residuals. MAX-block medium was used for blocking for 1 hour and then 5 µg/mL primary antibody diluted in MAXbinding medium was incubated with the sample at 4°C overnight (or 37°C for 2 hours). Next day, 5 µg/mL fluorescently labelled secondary antibody was used at room temperature for 1 hour. After completely washing out unbound antibodies, samples were proceeded with the anchoring and expansion steps.

Post-expansion antibody staining

For post-expansion antibody staining, gelled specimens were treated with the LysC-based digestion (in S3E and S7C Figs in [S1 File](#)) or heat-based SDS denaturation (in S3 Fig in [S1 File](#)), then followed by expansion [3]. Then the samples were incubated with 5 µg/mL primary antibody diluted in MAXbind staining medium at 4°C overnight (or 37°C for 2 hours) and washed with MAXwash medium four times. 5 µg/mL fluorescently labelled secondary antibody was incubated with the sample to develop signals before DAPI counterstaining and expansion.

Staining for lipids and carbohydrates

R18, FM and BODIPY were all tested for pre- and post-expansion staining. The working concentration for these dyes was chosen to be 10 µg/mL (diluted with fresh PBS). For pre-

expansion staining, lipid tags were introduced right before the gelation step in which samples were stained for 1–2 hours at room temperature. Then the samples were anchored with GMA at 4°C overnight, followed by incubation at room temperature for another 3 hours, digestion (proK-based) and expansion. For post-expansion staining, samples were fixed with 3% PFA/0.1% GA, and then anchored with GMA. The samples were digested with proK or LysC (for WGA staining), followed by expansion. After expansion, the samples were stained with antibodies or HCR-FISH first (if at all), and then with lipid tags or WGA-A647 for 1–2 hours at room temperature. The working concentration for WGA-A647 was chosen to be 5 µg/mL. Residual dyes were washed off with 1% Zwittergent in DPBS.

Expansion fluorescence *in situ* hybridization (ExFISH)

For ExFISH experiments (in Fig 1B, S3, S6, S10B Figs in S1 File) expanded gels were re-embedded in 3% AA-based (plus 0.15% BIS, 5 mM Tris base pH 9, and 0.05% APS/TEMED), non-expandable gel to maintain rigidity. With the re-embedding step, the expansion factor would decrease to ~3.2 compared to the original expansion factor of ~4.2. Two stacked #1.5 coverslips were usually used as the spacers between two glass slides for re-embedding. The HCR-FISH probes and reagents were purchased from Molecular Instruments, Inc. In general, the gel was incubated with hybridization buffer at room temperature for 30 min, and then with 1:500 diluted gene-specific probe (8 nM total final probe concentration) set at 37°C overnight. Next day, the gel was washed with HCR washing buffer at 37°C for 4 × 30 min and with 5× SSCT buffer (5× SSC buffer containing 0.1% Tween 20) at RT for 4 × 15 min, followed by incubation with 1:200 diluted, fluorescently labelled HCR hairpin amplifiers at room temperature overnight. Lastly, the gel was washed with 5× SSCT for 4 × 20 min and counterstained with 1 µg/mL DAPI. To characterize RNA capture efficiency by GMA, HCR-FISH against the same genes was performed in the same sample before and after anchoring. Before anchoring, HCR-FISH was done in HeLa cells and then the hybridized probes were removed with 80% formamide. Then, ExFISH after GMA-based uniExM was done with the same sample, where the same cells were imaged in both conditions. Transcripts in single cells were counted using MATLAB scripts as developed before [32, 33].

Expansion Sequencing (ExSeq)

The detailed protocol for ExSeq was published previously and involves a multi-day procedure [21]. 87 target genes were chosen to differentiate two major cancer clones in the SA501 PDX line (full gene list is provided in S5 Table in S1 File) [34]. In brief, a re-embedded gel was passivated with 2 M ethanolamine, 150 mM EDC and NHS. Then the passivated gel was subjected to targeted ExSeq (tExSeq) or untargeted ExSeq (uExSeq). For tExSeq, padlock probes targeting specific mRNAs (in general, 12–16 probes per gene and 100 nM per padlock probe diluted in 2× SSC containing 20% formamide) were used to hybridize with the sample at 37°C overnight. Then the unhybridized probes were completely washed off with fresh hybridization buffer and the sample was treated with 1.25 U/µL PBCV-1 DNA ligase at 37°C overnight, followed by inactivation at 60°C for 20 min. Next, the successfully ligated padlock probes were rolling circle amplified with 1 U/µL phi29 DNA polymerase at 30°C overnight. As all padlock probes targeting the same gene bear a predetermined barcode, the identity of the mRNA can be read out by commercially available sequencing reagents (e.g., the Illumina MiSeq kit). In comparison, uExSeq utilizes randomized 8N oligonucleotide probes to hybridize with any potential RNA targets without prior sequence knowledge. After that, reverse transcription was performed *in situ* with 10 U/µL SSIV reverse transcriptase to generate cDNAs containing inosine. The cDNAs were later segmented to proper sizes with endonuclease V and circularized

with 3 U/ μ L CircLigase. Then the target mRNAs were digested away with RNase H. Such circularized cDNAs were subjected to rolling circle amplification and sequencing readout. For detailed working mechanism and protocols of tExSeq and uExSeq, please refer to our previous work [21].

We adapted the sequencing-by-synthesis chemistry for *in situ* 7-base readout using the Illumina MiSeq v3 kit with a modified protocol. To help the registration process, the re-embedded gel sample was adherent to bind-silane (1:250 diluted in 80% ethanol) processed glass surface with the same re-embedding monomer solution containing 1:100 diluted TetraSpeck microspheres. Before sequencing, the sample was first treated with 400 U/mL terminal transferase and 50 μ M ddNTP to block nonspecifically exposed 3' ends in DNA, and then hybridized with 2.5 μ M sequencing primer (5'-TCT CGG GAA CGC TGA AGA CGG C-3') in 4 \times SSC at 37°C for 1 hour. After 3 \times 10 min washing with fresh 4 \times SSC, the sample was incubated with the PR2 incorporation buffer (part of the MiSeq kit) for 2 \times 15 min. Then the sample was pre-incubated with 0.5 \times incorporation mix buffer (IMT of the MiSeq kit) supplemented with 1 \times Taq polymerase buffer and 2.5 mM magnesium chloride at RT for 2 \times 15 min. Then the sample was incubated with 0.5 \times IMT at 50°C for 10 min for one base elongation. After the elongation reaction, the sample was washed with PR2 containing 2% Zwittergent at 50°C for 2 \times 15 min followed by additional washing with PR2 at RT for 2 \times 15 min. Next, the sample was immersed in imaging buffer (SRE of the MiSeq kit) and subjected to imaging (elaborated in the following section). After imaging, the sample was briefly washed with PR2 at RT for 2 \times 10 min. Then the sample was incubated with cleavage solution (EMS of the MiSeq kit) at 37°C for 3 \times 15 min. Lastly, the sample was washed with PR2 at 37°C for 2 \times 15 min and at RT for 2 \times 15 min, and then started with the next round of elongation process.

Data analysis for ExSeq

Data analysis for the sequenced PDX sample followed our established ExSeq processing pipeline (available at: <https://github.com/dgoodwin208/ExSeqProcessing>). For the 87-gene probe set, a 7-base barcoding strategy with error correction capacity was adopted. Upon microscopic readout, the raw image files were stored in 16-bit HDF5 format and subjected to color correction, registration, segmentation, basecalling and alignment as done in our previous work [21], and then performed manual cell segmentation in 2D according to a max-Z projection of the DAPI staining channel using the VASTLite package (<https://lichtman.rc.fas.harvard.edu/vast/>). In total, 793,535 unique transcripts were detected for a population of 3,339 cells (with effective lateral resolution \sim 78 nm and axial resolution of \sim 160 nm). For gene function annotation we refer to The Human Protein Atlas (<https://www.proteinatlas.org>) or The Human Gene Database (<https://www.genecards.org>). The spatial maps of single transcripts or functional gene groups were generated with MATLAB scripts (for coordinates extraction) and ImageJ packages (for visualization).

For single-cell biostatistics analysis we utilized the R toolkit Seurat 4. Before analysis, we further pruned the dataset based on the counts per cell values, where cells with less than 50 counts or more than 3000 counts were filtered out and we ended up with 2,732 cells. Then we normalized the counts per cell by the median value from all the cells and performed a log transformation. To identify cell clusters, we applied both unsupervised and supervised approaches. In unsupervised clustering, PCA suggested a majority of cells could be classified into two groups using the expression of 30 genes automatically pulled out by PCA. With that, we decided to visualize these two cell groups based on the relative expression of these 30 genes (by correlating the percentages of the top and bottom 15 genes in each single cell with the color channel intensities of an RGB composite image). Therefore, for every cell, its closeness to

a particular group rather than an arbitrary binary classification was presented so that the transitional status of different tumor clones may be preserved. The gene list used for supervised clustering was selected based on the bulk RNA-seq expression data, in which a set of 15, out of 87, marker genes for each clone (Clone_ZNF24: *RNF146*, *DDX24*, *OAZ2*, *ZNF24*, *TXNLI*, *IDH2*, *SEPT4*, *CDCA7*, *CP*, *RAD21*, *WDR61*, *RBP1*, *COX5A*, *HSPE1*, *IER3IP1*; Clone_XIST: *XIST*, *CD44*, *FBXO32*, *LGALS1*, *ARC*, *HLA-A*, *HLA-C*, *S100A11*, *CTSV*, *SLC25A6*, *ANXA1*, *ARHGDI1*, *SQLE*, *B2M*, *NDUFS5*) in the SA501 PDX model was applied for the initial dimension reduction (to match the number of marker genes selected in unsupervised clustering). Afterwards, the major cell clusters were presented via uniform manifold approximation and projection (UMAP). To cross-check the agreement between unsupervised and supervised cell classification results, we randomly sampled 2,000 cells from the two tumor clones as annotated by either cell classification method, and determined if they were correctly assigned to the same clone by the other cell classification method (in unsupervised cell classification, a minimum level of 30% for the summed 15 marker gene counts to total gene counts was applied as the threshold for robust clone assignment).

Imaging and image analysis

All imaging experiments were performed on a spinning disk confocal microscope (Andor Dragonfly) equipped with a Zyla sCMOS 4.2 plus camera (pixel size 6.5 μm) or a CSU-W1 SoRa super-resolution spinning disk confocal microscope (Nikon). Six main lasers on Dragonfly were used: 405 nm (100 mW), 488 nm (150 mW), 561 nm (150 mW), 594 nm (100 mW), 637 nm (140 mW) and 685 nm (40 mW). For tiled scan of full-size brain slices (Fig 1B, i and S8 Fig in S1 File), a 10 \times objective lens was used. For other imaging experiments, a Nikon CFI Apochromat LWD Lambda S 40XC water immersion objective lens (working distance 0.6 mm, NA 1.15) was used together with the Zeiss Immersol medium (Refractive Index 1.3339). For ExSeq using Illumina Miseq reagents, the following bandpass filters were used: 705–845 nm for base “C” channel, 663–737 nm for base “A” channel, 575–590 nm for base “T” channel, 500–550 nm for base “G” channel. All channels used 200 ms as the exposure time except that base “G” used 400 ms exposure time. For the sequenced cancer tissue, a total of 12 \times 6 fields of view (FOV dimension in pre-expansion units: 104 \times 104 \times 62.5 μm^3) were captured.

For characterization of expansion in uniExM, HeLa cells stained with β -tubulin antibody and DAPI were used. The size of cells was represented by the largest diameter value from the microtubule staining image, and this measurement was performed on the same cells pre- and post-expansion. In parallel, the area and shape descriptors of cell nuclei were measured with ImageJ. The following four parameters were obtained:

$$\text{Circularity} = \frac{[\text{Area}]}{[\text{Perimeter}]^2}, \text{Aspect ratio} = \frac{[\text{Major axis}]}{[\text{Minor axis}]},$$

$$\text{Roundness} = 4 \times \frac{[\text{Area}]}{\pi \times [\text{Major axis}]^2}, \text{Solidity} = \frac{[\text{Area}]}{[\text{Convex area}]}.$$

Quantification of expansion errors was performed as previously described [2, 3]. In brief, HeLa cells were stained with β -tubulin antibody pre-expansion. The same cells were imaged both pre- and post-expansion, where the pre-expansion images were taken with a Nikon SoRa super-resolution microscope (\sim 1.8-time spatial resolution improvement over standard confocal microscopy). The obtained images were first histogram normalized and deconvolved in imageJ. Then non-rigid registration was performed using B-spline grids to capture potential non-uniformities between images.

For periodicity analysis of β II-spectrin, cultured neurons were stained pre-expansion. Then the cells were expanded and imaged. Segments of axon processes with more than 10 spectrin signal clusters (a signal cluster was defined as fluorescence intensity above 5 times of the standard deviation of the background level) were selected and relevant fluorescence profiles were extracted. The fluorescence traces in space were scaled back to the pre-expansion level and autocorrelation was performed in OriginLab software. From the obtained autocorrelation curve, periodicity was calculated by averaging the distances of the first four adjacent peaks.

Results and discussion

Epoxides as multifunctional anchors

We reasoned that an ideal multifunctional anchor for ExM should be chemically active, mechanistically predictable, and universally accessible. Epoxides fit this bill, and are already ubiquitous in daily life (e.g., in epoxy adhesives) and well understood. One study has explored polyepoxides as an intramolecular crosslinker to reduce molecular damage during harsh tissue treatments [12]. In our study, we use epoxy acrylates to directly link proteins and nucleic acids to a swellable hydrogel network permeating a specimen. The ring-opening process of epoxides is a nucleophilic substitution reaction and could follow two pathways: an S_N1 -like reaction under acidic conditions or an S_N2 reaction under basic conditions, making the anchoring reaction pH sensitive [35]. Acidic solutions are able to protonate epoxides and open the high-tension three-atom ring directly, resulting in rapid conjugation with weak nucleophiles such as water and alcohol [36]. However, acids could also protonate nucleophiles on the biomolecules or labels to be anchored. Hence, we chose a slightly basic system, well within the range of standard specimen treatments (pH = 8.5, buffered by 100 mM sodium bicarbonate NaHCO_3), for epoxides to react with nucleophiles of biological importance, including but not limited to cysteine, histidine, lysine, glutamic acid, tyrosine, and guanine (schematics in S2 Fig in S1 File) [12, 37, 38]. We chose for this paper to investigate glycidyl methacrylate (GMA), which contains an epoxide and a vinyl group, as an anchoring moiety. A high-level comparison of LabelX, MelphaX, and GMA with regards to key properties in application is summarized in S1 Table in S1 File.

We confirmed that uniExM is compatible with both a popular protein retention form of ExM (proExM) and an RNA retention form of ExM that supports *in situ* hybridization (ExFISH) (examples in S3 Fig in S1 File and Fig 1B, i). Specifically, 0.04% (w/v) GMA, as compared to an established method using 0.01% (w/v) LabelX plus an additional 0.005% (w/v) AcX [4], fared well, retaining native yellow fluorescent protein (YFP) intensity ~4 times stronger (Fig 1B, ii). The single-spot intensity of hybridization chain reaction (HCR)-FISH was 2 times stronger in GMA treated tissues (Fig 1B, ii), reminiscent of the improvement yielded by MelphaX over LabelX [27]. Both RNAs and proteins could be retained and visualized in the same specimen, after GMA anchoring, for both cultured cells and intact tissues (Fig 1B, iii); hence, we termed this simplified protocol united expansion microscopy (uniExM).

Characterization of uniExM distortion and yield

Perhaps because only the anchoring step was changed, without alteration of the gelation, softening, and expansion steps, the rest of the expansion process proceeded smoothly, without requiring further refinement. Not surprisingly, uniExM supported high-resolution imaging of fine structures, including microtubules in cultured HeLa cells (Fig 2A). The expansion factor was found to be 4.2–4.4 using 0.04% GMA (Fig 2A, iv) and the distortion incurred by expansion was similar to previously published results, a few percent over a field of view of a few tens of microns (benchmarked against Nikon SoRa super-resolution microscopy) (Fig 2A, v). In

addition, the morphology and geometry of the nucleus was reliably maintained after expansion (S4 Fig in [S1 File](#)).

As with HCR-FISH before it, uniExM is able to decrowd densely packed RNA molecules for better detection ([Fig 2B, i](#)). To gauge how uniExM facilitates retention of RNA molecules, we systematically varied GMA concentration, reaction pH, and temperature, evaluating the retention of three highly expressed genes (*GAPDH*, *EEF1A1*, *ACTB*) (S5 Fig in [S1 File](#)). The optimal reaction condition was determined to be 0.04% GMA for cultured cells at pH 8.5 (100 mM NaHCO₃), at room temperature. For tissue samples we used 0.1% GMA to ensure sufficient anchoring of multiple types of biomolecules, and found in practice that increased temperature (*e.g.*, from room temperature to 37°C) could facilitate the diffusion and anchoring efficiency of epoxide, consistent with previous reports [4, 6]. Moreover, we demonstrated that the anchoring reaction could be efficiently controlled by varying temperature and pH; at 4°C and neutral pH, the anchoring efficiency for RNA can be suppressed by more than 50% after 12 h incubation (termed reaction “Off” condition), while it can be rapidly recovered to full efficacy by an additional 3 h incubation at 25°C and pH 8.5 (termed reaction “On” condition) (S5D Fig in [S1 File](#)).

We quantified three moderately expressed genes (*TOP2A*, *TFRC*, *USF2*) with HCR-FISH before vs. after GMA anchoring. uniExM preserved RNA molecules with ~100% retention efficiency ([Fig 2B, ii, iii](#)). As another comparison, GMA was equal to, or perhaps even slightly better, than LabelX in preservation of highly expressed mRNA targets (S6 Fig in [S1 File](#)). Thus, both in terms of supporting even expansion, and high yield of target, GMA is an excellent unified anchor for both proteins and RNAs.

uniExM for preservation of protein content and ultrastructure

We next explored applications of uniExM in different biological contexts. We chose β II-spectrin in neurons to image, since its periodic distribution in axons was discovered via super-resolution imaging [39, 40]. In cultured mouse hippocampal neurons, the periodic distribution of β II-spectrin was prevalently observed in axons ([Fig 3A](#); more examples in S7A Fig in [S1 File](#)). The distance between two adjacent β II-spectrin spots was found to be ~190 nm ([Fig 3B](#)), as reported earlier [39], while this periodicity was not apparent in pre-expansion samples. The periodic distribution of β II-spectrin can be additionally visualized with an autocorrelation analysis ([Fig 3C](#)), which we performed with a 7 \times expansion protocol based on the TReX protocol [26]. Different expansion factors can be obtained by tuning the cross-linker concentration of the expansion microscopy hydrogel; here we simply show the compatibility of our new anchoring strategy with the tuning of hydrogel expansion factor. Finally, autocorrelation analyses from four independent samples were performed, yielding calculated periodicity values (193 ± 15 nm for 4 \times expanded cells, 187 ± 10 nm for 7 \times expanded cells, values reported as mean \pm standard deviation) consistent with results previously obtained by super-resolution STORM or STED imaging ([Fig 3D](#) and S7B Fig in [S1 File](#)) [41, 42]. Moreover, post-expansion antibody staining revealed the same spatial pattern of β II-spectrin in both 4 \times and 7 \times expanded cells ([Fig 3E](#) and S7C Fig in [S1 File](#)). Post-expansion staining is increasingly popular because expanding proteins away from each other, and then staining them, can make more room for antibodies to bind to their targets [25]; here, we simply show compatibility of our new anchoring strategy with post-expansion staining.

Polyepoxides, which can crosslink multiple biomolecules to each other, and even multiple parts of a biomolecule to each other, have been shown to help proteins such as fluorescent proteins retain function in tissue specimens under harsh conditions, such as high heating [12]. High heat treatment of hydrogel-embedded tissues is a popular softening method to precede

an expansion step, because it preserves epitopes for post-expansion staining, which can result in better access to epitopes than pre-expansion staining [25, 43]. However, the high heat treatment can destroy the fluorescence of GFP, amongst other sensitive moieties. We combined GMA with a polyepoxide, trimethylolpropane triglycidyl ether (TMPTE), to assess the performance of this cocktail in preservation of fluorescent protein function after heat-based tissue softening. We tested two tissue processing protocols requiring heating above 50°C: the SDS-based sample denaturation (95°C for 1h) [25] and the proK-based enzymatic digestion (60°C for 2h) [44]. Compared with LabelX plus AcX, GMA plus TMPTE showed better retention of fluorescence signals for paraformaldehyde (PFA)-perfused, fresh frozen Thy1-YFP mouse brain slices (~440% signal improvement for SDS-based denaturation; 250% signal improvement for proK-based digestion; S8 Fig in [S1 File](#)).

uniExM for *in situ* sequencing of RNA

Expansion microscopy greatly facilitates *in situ* sequencing, enabling multiplexed RNA analysis with high spatial precision; we named the optimized combination expansion sequencing (ExSeq) [21]. In untargeted ExSeq, linear probes containing randomized octamer sequences are hybridized to RNA targets, followed by reverse transcription of adjacent RNA sequence information into cDNA form. cDNAs are then circularized and undergo rolling circle amplification (RCA) (schematized in S9 Fig in [S1 File](#)). Then, in each round of sequencing readout, the bases being added are imaged through fluorescence microscopy (example in S10A Fig in [S1 File](#)). In addition to untargeted ExSeq, one can perform targeted ExSeq against sets of specific RNAs ([Fig 4A](#)), by bringing in padlock probes that hybridize to targets, and then sequencing barcodes found on the padlock probes (schematized in S9 Fig in [S1 File](#); example in S10B Fig in [S1 File](#)). Comparing amplicons (containing amplified barcode sequences) from targeted ExSeq using GMA, to spots seen with classical HCR-FISH, showed excellent agreement in spot counts ([Fig 4B, i](#)). The sequencing, conveniently, can be done with standard Illumina MiSeq sequencing-by-synthesis (SBS) reagents ([Fig 4B, ii](#)). We performed sequencing of barcodes on padlock probes targeting *ACTB* mRNAs to test the stability of uniExM-based ExSeq across multiple rounds of sequencing in mouse brain tissues. The padlock probes used contained repetitive “T” bases in their barcode region, so the amplicons should emit the same fluorescence signal in each round of sequencing. The amplicons were first examined with a universal detection probe to generate a reference image, then three consecutive rounds of sequencing were performed (S10C Fig in [S1 File](#)). Amplicons were consistently detected in each round (with an average detection rate of ~96.5% across 20 fields of view from 2 different mouse brains), indicating that uniExM-based ExSeq is compatible with the full SBS chemistry cycle (*i. e.*, elongation, detection and cleavage steps). Moreover, Thy1-YFP positive structures in the mouse brain tissues (*e.g.*, dendrites and spines) were consistently detected after the ExSeq library preparation procedure (as seen by comparing images from the YFP channel before vs. after library preparation), helpful for analyzing transcriptomics in the context of morphological compartments like synapses and axons.

We performed 7-round SBS to profile 87 genes known to classify tumor cells into subclasses in SA501 breast cancer PDX tissues [30] (the original LabelX-based ExSeq was demonstrated for 4 rounds of SBS). Importantly, uniExM significantly reduces the cost of ExSeq, as the anchoring reagent contributes to more than half of the entire cost of the original protocol (see S1 Table in [S1 File](#) for more details). In a $1.24 \times 0.62 \text{ mm}^2$ region of interest, 793,535 raw reads (colored by function annotations) and 3,339 cells in total were detected ([Fig 4C, ii](#) and S10D Fig in [S1 File](#)). Many kinds of analysis are possible: in [Fig 4C, iii](#), transcripts from three functional groups were presented as 8-bit “RGB” images where the color intensity reflected the

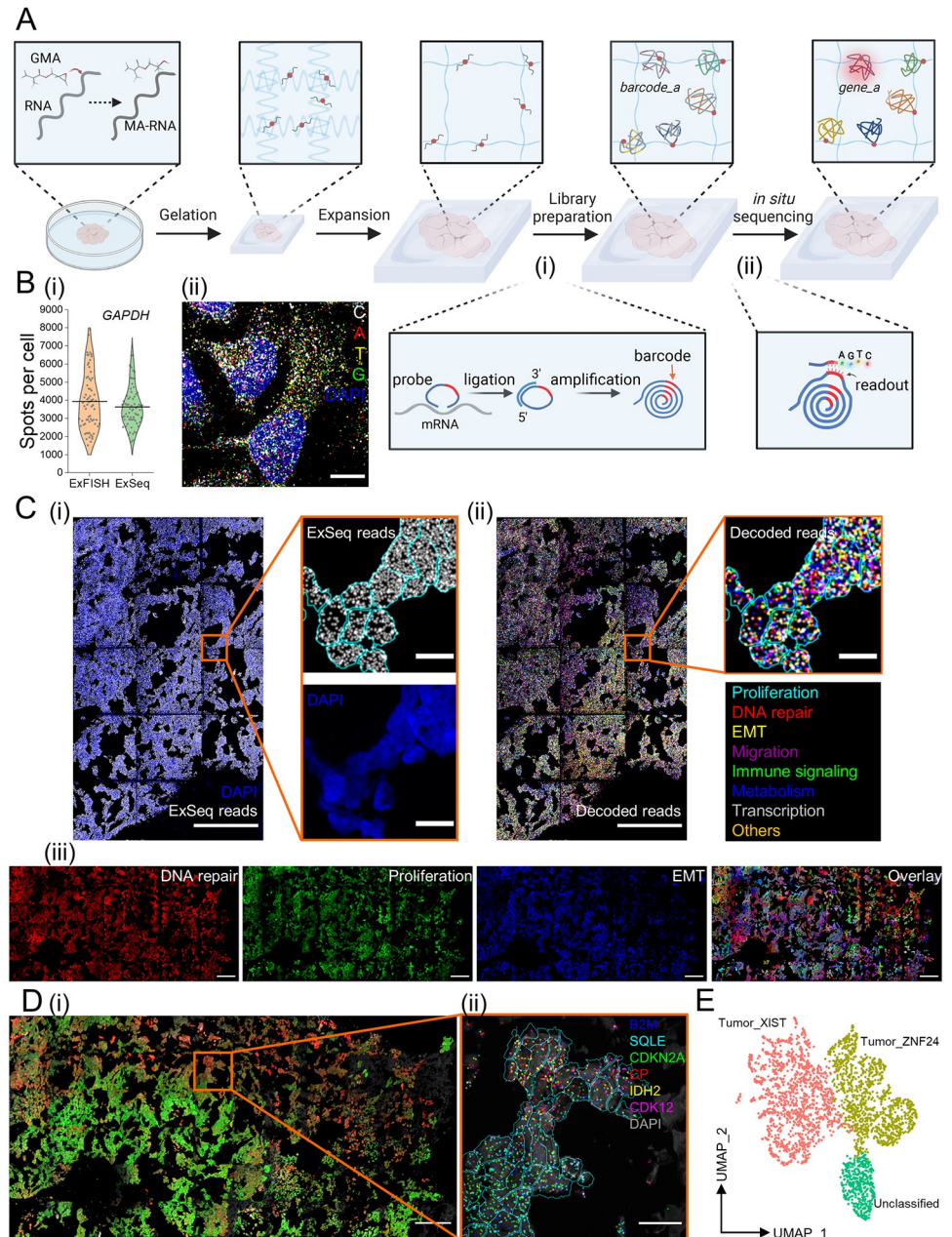


Fig 4. uniExM-supported *in situ* RNA sequencing (ExSeq). (A) Schematic of the workflow for targeted ExSeq (tExSeq): target RNA molecules are reacted with GMA to acquire methacrylate groups (termed MA-RNA) and anchored to the expandable hydrogel. Padlock probes are then introduced to hybridize with the target RNAs in the expanded biological sample. Upon successful hybridization, the sequence of a target mRNA serves as a “splint” for PBCV-1 enzyme-mediated ligation of the bound padlock, as shown in the zoomed-in panel (i). Afterwards, rolling circle amplification (RCA) is applied to amplify the ligated probes that harbor barcodes specific to targets. Finally, the barcodes are read out by *in situ* sequencing chemistry, as shown in the zoomed-in panel (ii). The full readout of a specific barcode can then be used to reveal the gene identity (e.g., from barcode_a to gene_a) together with its location information. In such way, multiple gene targets can be decoded (represented as differentially colored amplicons). (B) Validation of ExSeq enzymatics and sequencing-by-synthesis (SBS) chemistry in samples processed with the uniExM procedure. (i) *GAPDH* in HeLa cells was chosen to undergo HCR-FISH or tExSeq. The numbers of detected signal spots per cell were quantitatively compared. No statistically significant difference was observed between the two methods. (Data shown as violin plots, with raw data points presented, and mean values highlighted with solid lines; $n = 70$ cells from 4 samples, 2 culture batches; two-sample t -test was performed with $p > 0.1$) (ii) A fluorescence image showing raw ExSeq signals from all four base channels in HeLa cells undergoing targeted ExSeq. Scale bars (in pre-expansion units): 20 μm . (C) Demonstration of ExSeq applying an 87-gene panel in GMA-anchored SA501 PDX

breast cancer tissue. (i) Overview of the raw ExSeq reads (gray spots) in the tissue. DAPI staining for nuclei was used for cell segmentation and reads assignment (shown in the zoomed-in images). (ii) The raw ExSeq reads were decoded and colored based on 8 distinct gene function groups (full list in S5 Table in S1 File). Scale bars (in pre-expansion units): 100 μm (for stitched overview images), 10 μm (for zoomed-in images). (iii) Gene maps of 3 selected function groups—DNA repair, proliferation and epithelial-mesenchymal transition (EMT), were used to help visualize heterogeneity of cell status in the whole tissue. The decoded transcripts of genes belonging to each functional group were summed and their ratio to total transcript counts were assigned to the “R”, “G”, “B” color channels of the image, respectively. During the color assigning process, a scaling factor of 3.33 (for DNA repair and proliferation) or 2.5 (for EMT) was introduced; that is, if the EMT group of genes was 40% of the total transcripts in one cell, its assigned “B” channel was given the maximum color intensity ($40\% \times 2.5 = 100\%$). Then, the three individual channels were combined to make a composite image (right). Scale bars (in pre-expansion units): 100 μm . Linear expansion factor: 3.2 (the expanded gel was re-embedded before sequencing). (D) Unsupervised principal component analysis (PCA) identified two primary gene groups for cell classification. (i) Using these two PCA gene groups, a distribution of different cancer cells was revealed. In this presented image, the summed transcripts of each PCA group normalized to the total transcript count for a given cell were assigned to the “R” channel and “G” channel, respectively (scaling factor: 3.33). Then the two images were overlaid to make a composite. Scale bar (in pre-expansion units): 100 μm . (ii) In the zoomed-in region where differentially colored cells co-exist, 6 marker genes are plotted; their distribution varies across cells in the subregion. Scale bar (in pre-expansion units): 10 μm . (E) Uniform manifold approximation and projection (UMAP) representation of the cell typing results using bulk RNA-seq identified marker genes in the SA501 cancer model. According to the panel design, the 87 gene list could differentiate two primary cancer cell clones that are successfully annotated on UMAP—“Tumor_XIST” and “Tumor_ZNF24”, named after their feature genes. A small group of cells are marked as “Unclassified”, likely attributed to non-cancer interstitial or other cells.

<https://doi.org/10.1371/journal.pone.0291506.g004>

overall expression level of the members of that group in each individual cell. Principal component analysis (PCA), applied to all the cells of the sample, revealed two distinct cell groups distinguished by 30 out of the 87 genes (S10E Fig in S1 File). Based on the expression levels of these two PCA-generated gene sets, we assigned a color code to each individual cell (Fig 4D, i). The summed counts of each PCA group-specific gene set (15 genes), normalized to the total count in each individual cell, were then plotted as the red and green channels of the “RGB” image, respectively. The composite image shows a spatially varying distribution of the colored cells in space, explicitly delineating two tumor cell populations. In a zoomed-in region where cells of both groups were present, transcripts from distinct PCA lists were detected in different cells (Fig 4D, ii). As a second method of analysis, we ran a dimensionality reduction algorithm using the clone-specific marker genes with significant differential expression from the RNA-seq data of the same PDX model [34] and presented the results with UMAP, where two tumor cell clones (denoted as “Tumor_XIST” and “Tumor_ZNF24”) and one group of “Unclassified” cells were identified (Fig 4E). These two classified groups of cells well correspond to the bright-green and bright-red colored cells in Fig 4D, i, respectively. In detail, comparing the unsupervised and supervised results, 85.1% of tumor clone cells annotated by the supervised method were classified as the same clone by unsupervised method, whereas 82.7% of cells classified by the unsupervised method were cross-verified by the supervised method. In this demonstration, starting from a marker list selected either by unsupervised PCA or supervised RNA-seq data, highly consistent tumor clone identification was obtained. These orthogonal analyses not only help support the validity of the biological findings but also reflect the robustness of our technology.

uniExM for multimodal detection beyond proteins and nucleic acids

Our focus here was the retention of proteins and RNAs with a single anchor during ExM. Without seeking to make broad quantitative claims about the efficacy of doing so, we did examine at a qualitative level the compatibility of uniExM with commercially available lipid stains and markers of carbohydrates. We selected three lipid stains—octadecyl rhodamine B chloride (R18), FM 1-43FX (FM) and BODIPY FL C₁₂ (BODIPY), all of which showed signals in lipid-rich or membranous structures (S11A, S11B Fig in S1 File), consistent with their

staining patterns in unexpanded samples (S12A Fig in [S1 File](#)). In addition, GMA treated cells showed significantly stronger lipid staining signals than AcX treated cells (S12B Fig in [S1 File](#)). Using Alexa647 tagged wheat germ agglutinin (WGA), which binds *N*-acetylglucosamine (GlcNAc), we were able to see specific signals in nuclear membranes of cultured HeLa cells and blood vessels of mouse brain tissues (S11C and S13 Figs in [S1 File](#)). Notably, as WGA can specifically bind to glycoprotein-enriched nucleoporins (a key component of the nuclear pore complex) [45, 46], GMA efficiently detected putative nucleoporin puncta on nuclear membranes in the context of uniExM (S12C Fig in [S1 File](#)). Such stains could potentially be used together, in the same specimen, along with antibody stains and FISH probes, supporting multimodal imaging of many kinds of biomolecule in the same cell or tissue section (S13 Fig in [S1 File](#)).

Conclusions

Here we show that a single anchoring molecule can support the expansion of both proteins and RNAs away from each other in expansion microscopy, reducing the complexity and cost compared to earlier anchoring strategies, which required different anchors for different kinds of biomolecules. We used an epoxide, an inexpensive and highly reactive moiety capable of binding to many kinds of biomolecules, that contained a vinyl group capable of participating in polymerization. We found this molecule, GMA, to enable good retention of proteins and RNAs, and to support labeling for visualization of other biomolecules, although more work will be required to quantitatively validate the latter in multiple cell and tissue types.

Past anchoring strategies for ExM have used different anchors for different kinds of biomolecules, *e.g.*, using an aldehyde or NHS ester to bind amines on proteins, or an alkylating reagent to bind guanine on RNA. The latter strategy requires end users to mix multiple chemicals overnight to create the anchor, and some protocols administer different anchors in separate steps. Here, no end user synthesis is needed, and only a single step is needed to add the multimodal anchor GMA.

We demonstrated the utility of this united ExM, or uniExM, protocol in cells and tissues. Perhaps because of the rest of the protocol is unaltered compared to previous ExM protocols, we saw no differences in the performance of the rest of the protocol (*e.g.*, distortion, resolution). uniExM was able to support not just classical ExM protocols like antibody detection of proteins and FISH detection of RNAs, but also our recently published ExSeq protocol for multiplexed visualization of RNAs. In short, uniExM will find utility in a variety of contexts in biology.

Supporting information

S1 File. Document containing S1–S13 Figs and S1–S5 Tables.
(DOCX)

Acknowledgments

We acknowledge Asmamaw T. Wassie, Yixi Liu, Ruihan Zhang and other Boyden lab members for insightful discussions.

List of IMAXT Grand Challenge Consortium investigators:

Greg Hannon, Cancer Research UK Cambridge Institute (Lead author, Greg.Hannon@cruk.cam.ac.uk)

Shankar Balasubramanian, Cancer Research UK Cambridge Institute

Bernd Bodenmiller, University of Zurich

Carlos Caldas, Cancer Research UK Cambridge Institute
Dario Bressan, Cancer Research UK Cambridge Institute
Johanna Joyce, University of Lausanne
Nicholas Walton, University of Cambridge
Owen Harris, Suil Interative Ltd
Sam Aparicio, The University of British Columbia
Simon Tavare, Cancer Research UK Cambridge Institute
Xiaowei Zhuang, Harvard University
Ed Boyden, Massachusetts Institute of Technology
Sohrab Shah, The University of British Columbia

Author Contributions

Conceptualization: Yi Cui, Gaojie Yang, Edward S. Boyden.

Data curation: Yi Cui, Gaojie Yang, Daniel R. Goodwin, Ciara H. O’Flanagan, Anubhav Sinha, Chi Zhang, Tay Won Shin.

Formal analysis: Yi Cui, Gaojie Yang, Daniel R. Goodwin.

Funding acquisition: Samuel Aparicio, Edward S. Boyden.

Investigation: Yi Cui, Gaojie Yang, Ciara H. O’Flanagan, Edward S. Boyden.

Methodology: Yi Cui, Gaojie Yang, Edward S. Boyden.

Project administration: Edward S. Boyden.

Resources: Demian Park, Edward S. Boyden.

Software: Yi Cui, Daniel R. Goodwin.

Supervision: Samuel Aparicio, Edward S. Boyden.

Validation: Yi Cui, Gaojie Yang, Chi Zhang, Kristina E. Kitko.

Visualization: Yi Cui, Gaojie Yang.

Writing – original draft: Yi Cui, Edward S. Boyden.

Writing – review & editing: Yi Cui, Edward S. Boyden.

References

1. Sahl SJ, Hell SW, Jakobs S. Fluorescence nanoscopy in cell biology. *Nat Rev Mol Cell Biol.* 2017; 18(11):685–701. <https://doi.org/10.1038/nrm.2017.71> PMID: 28875992
2. Chen F, Tillberg PW, Boyden ES. Expansion microscopy. *Science.* 2015; 347(6221):543–8.
3. Tillberg PW, Chen F, Piatkevich KD, Zhao Y, Yu CC, English BP, et al. Protein-retention expansion microscopy of cells and tissues labeled using standard fluorescent proteins and antibodies. *Nat Biotechnol.* 2016; 34(9):987–92. <https://doi.org/10.1038/nbt.3625> PMID: 27376584
4. Chen F, Wassie AT, Cote AJ, Sinha A, Alon S, Asano S, et al. Nanoscale imaging of RNA with expansion microscopy. *Nat Methods.* 2016; 13(8):679–84. <https://doi.org/10.1038/nmeth.3899> PMID: 27376770
5. Wassie AT, Zhao Y, Boyden ES. Expansion microscopy: principles and uses in biological research. *Nat Methods.* 2019; 16(1):33–41. <https://doi.org/10.1038/s41592-018-0219-4> PMID: 30573813
6. Asano SM, Gao R, Wassie AT, Tillberg PW, Chen F, Boyden ES. Expansion microscopy: protocols for imaging proteins and RNA in cells and tissues. *Curr Protoc Cell Biol.* 2018; 80(1):e56. <https://doi.org/10.1002/cpcb.56> PMID: 30070431

7. Chozinski TJ, Halpern AR, Okawa H, Kim HJ, Tremel GJ, Wong RO, et al. Expansion microscopy with conventional antibodies and fluorescent proteins. *Nat Methods*. 2016; 13(6):485–8. <https://doi.org/10.1038/nmeth.3833> PMID: 27064647
8. Ku T, Swaney J, Park JY, Albanese A, Murray E, Cho JH, et al. Multiplexed and scalable super-resolution imaging of three-dimensional protein localization in size-adjustable tissues. *Nat Biotechnol*. 2016; 34(9):973–81. <https://doi.org/10.1038/nbt.3641> PMID: 27454740
9. Zhao Y, Bucur O, Irshad H, Chen F, Weins A, Stancu AL, et al. Nanoscale imaging of clinical specimens using pathology-optimized expansion microscopy. *Nat Biotechnol*. 2017; 35(8):757–64. <https://doi.org/10.1038/nbt.3892> PMID: 28714966
10. Chang JB, Chen F, Yoon YG, Jung EE, Babcock H, Kang JS, et al. Iterative expansion microscopy. *Nat Methods*. 2017; 14(6):593–9. <https://doi.org/10.1038/nmeth.4261> PMID: 28417997
11. Freifeld L, Odstrcil I, Forster D, Ramirez A, Gagnon JA, Randlett O, et al. Expansion microscopy of zebrafish for neuroscience and developmental biology studies. *Proc Natl Acad Sci U S A*. 2017; 114(50):E10799–E808. <https://doi.org/10.1073/pnas.1706281114> PMID: 29162696
12. Park YG, Sohn CH, Chen R, McCue M, Yun DH, Drummond GT, et al. Protection of tissue physico-chemical properties using polyfunctional crosslinkers. *Nat Biotechnol*. 2018; 37(1):73–+. <https://doi.org/10.1038/nbt.4281> PMID: 30556815
13. Gao R, Asano SM, Upadhyayula S, Pisarev I, Milkie DE, Liu TL, et al. Cortical column and whole-brain imaging with molecular contrast and nanoscale resolution. *Science*. 2019; 363(6424). <https://doi.org/10.1126/science.aau8302> PMID: 30655415
14. Truckenbrodt S, Sommer C, Rizzoli SO, Danzl JG. A practical guide to optimization in X10 expansion microscopy. *Nat Protoc*. 2019; 14(3):832–63. <https://doi.org/10.1038/s41596-018-0117-3> PMID: 30778205
15. Gambarotto D, Zwettler FU, Le Guennec M, Schmidt-Cernohorska M, Fortun D, Borgers S, et al. Imaging cellular ultrastructures using expansion microscopy (U-ExM). *Nat Methods*. 2019; 16(1):71–4. <https://doi.org/10.1038/s41592-018-0238-1> PMID: 30559430
16. Karagiannis ED, Kang JS, Shin TW, Emenari A, Asano S, Lin L, et al. Expansion microscopy of lipid membranes. *bioRxiv*. 2019:829903.
17. M'Saad O, Bewersdorf J. Light microscopy of proteins in their ultrastructural context. *Nat Commun*. 2020; 11(1):3850. <https://doi.org/10.1038/s41467-020-17523-8> PMID: 32737322
18. Yu CJ, Barry NC, Wassie AT, Sinha A, Bhattacharya A, Asano S, et al. Expansion microscopy of *C. elegans*. *Elife*. 2020; 9:e46249. <https://doi.org/10.7554/eLife.46249> PMID: 32356725
19. Wen G, Vanheusden M, Acke A, Valli D, Neely RK, Leen V, et al. Evaluation of direct grafting strategies via trivalent anchoring for enabling lipid membrane and cytoskeleton staining in expansion microscopy. *ACS Nano*. 2020; 14(7):7860–7. <https://doi.org/10.1021/acsnano.9b09259> PMID: 32176475
20. Gao R, Yu CJ, Gao L, Piatkevich KD, Neve RL, Munro JB, et al. A highly homogeneous polymer composed of tetrahedron-like monomers for high-isotropy expansion microscopy. *Nat Nanotechnol*. 2021; 16(6):698–707. <https://doi.org/10.1038/s41565-021-00875-7> PMID: 33782587
21. Alon S, Goodwin DR, Sinha A, Wassie AT, Chen F, Daugharthy ER, et al. Expansion sequencing: Spatially precise in situ transcriptomics in intact biological systems. *Science*. 2021; 371(6528):eaax2656. <https://doi.org/10.1126/science.aax2656> PMID: 33509999
22. Sun DE, Fan X, Shi Y, Zhang H, Huang Z, Cheng B, et al. Click-ExM enables expansion microscopy for all biomolecules. *Nat Methods*. 2021; 18(1):107–13. <https://doi.org/10.1038/s41592-020-01005-2> PMID: 33288959
23. Shi X, Li Q, Dai Z, Tran AA, Feng S, Ramirez AD, et al. Label-retention expansion microscopy. *J Cell Biol*. 2021; 220(9):e202105067. <https://doi.org/10.1083/jcb.202105067> PMID: 34228783
24. Liu J, Fang X, Liu Z, Li R, Yang Y, Sun Y, et al. Expansion microscopy with multifunctional polymer dots. *Adv Mater*. 2021; 33(25):e2007854. <https://doi.org/10.1002/adma.202007854> PMID: 33988880
25. Sarkar D, Kang J, Wassie AT, Schroeder ME, Peng Z, Tarr TB, et al. Revealing nanostructures in brain tissue via protein decrowding by iterative expansion microscopy. *Nat Biomed Eng*. 2022; 6(9):1057–73. <https://doi.org/10.1038/s41551-022-00912-3> PMID: 36038771
26. Damstra HGJ, Mohar B, Eddison M, Akhmanova A, Kapitein LC, Tillberg PW. Visualizing cellular and tissue ultrastructure using Ten-fold Robust Expansion Microscopy (TREx). *Elife*. 2022; 11:e73775. <https://doi.org/10.7554/eLife.73775> PMID: 35179128
27. Wang Y, Eddison M, Fleishman G, Weigert M, Xu S, Wang T, et al. EASI-FISH for thick tissue defines lateral hypothalamus spatio-molecular organization. *Cell*. 2021; 184(26):6361–77 e24. <https://doi.org/10.1016/j.cell.2021.11.024> PMID: 34875226
28. Cho I, Chang JB. Simultaneous expansion microscopy imaging of proteins and mRNAs via dual-ExM. *Sci Rep*. 2022; 12(1):3360. <https://doi.org/10.1038/s41598-022-06903-3> PMID: 35233025

29. Klimas A, Gallagher BR, Wijesekara P, Fekir S, DiBernardo EF, Cheng Z, et al. Magnify is a universal molecular anchoring strategy for expansion microscopy. *Nat Biotechnol*. 2023;1–12.
30. Eirew P, Steif A, Khattra J, Ha G, Yap D, Farahani H, et al. Dynamics of genomic clones in breast cancer patient xenografts at single-cell resolution. *Nature*. 2015; 518(7539):422–6. <https://doi.org/10.1038/nature13952> PMID: 25470049
31. Zhang C, Kang JS, Asano SM, Gao R, Boyden ES. Expansion microscopy for beginners: visualizing microtubules in expanded cultured HeLa cells. *Curr Protoc Neurosci*. 2020; 92(1):e96. <https://doi.org/10.1002/cpns.96> PMID: 32497404
32. Cui Y, Hu D, Markillie LM, Chrisler WB, Gaffrey MJ, Ansong C, et al. Fluctuation localization imaging-based fluorescence in situ hybridization (fliFISH) for accurate detection and counting of RNA copies in single cells. *Nucleic Acids Res*. 2018; 46(2):e7. <https://doi.org/10.1093/nar/gkx874> PMID: 29040675
33. Cui Y, Melby ES, Mensch AC, Laudadio ED, Hang MN, Dohnalkova A, et al. Quantitative mapping of oxidative stress response to lithium cobalt oxide nanoparticles in single cells using multiplexed in situ gene expression analysis. *Nano Lett*. 2019; 19(3):1990–7. <https://doi.org/10.1021/acs.nanolett.8b05172> PMID: 30773885
34. Campbell KR, Steif A, Laks E, Zahn H, Lai D, McPherson A, et al. clonealign: statistical integration of independent single-cell RNA and DNA sequencing data from human cancers. *Genome Biol*. 2019; 20(1):54. <https://doi.org/10.1186/s13059-019-1645-z> PMID: 30866997
35. Parker R-E, Isaacs N. Mechanisms of epoxide reactions. *Chem Rev*. 1959; 59(4):737–99.
36. Hansen T, Vermeeren P, Haim A, van Dorp MJ, Codée JD, Bickelhaupt FM, et al. Regioselectivity of epoxide ring-openings via SN2 reactions under basic and acidic conditions. *Eur J Org Chem*. 2020; 2020(25):3822–8.
37. Chen G, Heim A, Riether D, Yee D, Milgrom Y, Gawinowicz MA, et al. Reactivity of functional groups on the protein surface: development of epoxide probes for protein labeling. *J Am Chem Soc*. 2003; 125(27):8130–3. <https://doi.org/10.1021/ja034287m> PMID: 12837082
38. Richter S, Gatto B, Fabris D, Takao K, Kobayashi S, Palumbo M. Clerocidin alkylates DNA through its epoxide function: evidence for a fine tuned mechanism of action. *Nucleic Acids Res*. 2003; 31(17):5149–56. <https://doi.org/10.1093/nar/gkg696> PMID: 12930966
39. Xu K, Zhong G, Zhuang X. Actin, spectrin, and associated proteins form a periodic cytoskeletal structure in axons. *Science*. 2013; 339(6118):452–6. <https://doi.org/10.1126/science.1232251> PMID: 23239625
40. He J, Zhou R, Wu Z, Carrasco MA, Kurshan PT, Farley JE, et al. Prevalent presence of periodic actin-spectrin-based membrane skeleton in a broad range of neuronal cell types and animal species. *Proc Natl Acad Sci U S A*. 2016; 113(21):6029–34. <https://doi.org/10.1073/pnas.1605707113> PMID: 27162329
41. Sidenstein SC, D'Este E, Bohm MJ, Danzl JG, Belov VN, Hell SW. Multicolour multilevel STED nanoscopy of actin/spectrin organization at synapses. *Sci Rep*. 2016; 6:26725. <https://doi.org/10.1038/srep26725> PMID: 27220554
42. Martinez GF, Gazal NG, Quassollo G, Szalai AM, Cid-Pellitero ED, Durcan TM, et al. Quantitative expansion microscopy for the characterization of the spectrin periodic skeleton of axons using fluorescence microscopy. *Sci Rep*. 2020; 10(1):2917. <https://doi.org/10.1038/s41598-020-59856-w> PMID: 32076054
43. Valdes PA, Yu C-C, Aronson J, Zhao Y, Bernstock JD, Bhere D, et al. Decrowding expansion pathology: unmasking previously invisible nanostructures and cells in intact human brain pathology specimens. *bioRxiv*. 2021.
44. Rao MB, Tanksale AM, Ghatge MS, Deshpande VV. Molecular and biotechnological aspects of microbial proteases. *Microbiol Mol Biol Rev*. 1998; 62(3):597–635. <https://doi.org/10.1128/MMBR.62.3.597-635.1998> PMID: 9729602
45. D'Angelo MA, Anderson DJ, Richard E, Hetzer MW. Nuclear pores form de novo from both sides of the nuclear envelope. *Science*. 2006; 312(5772):440–3. <https://doi.org/10.1126/science.1124196> PMID: 16627745
46. Shi KY, Mori E, Nizami ZF, Lin Y, Kato M, Xiang S, et al. Toxic PRn poly-dipeptides encoded by the C9orf72 repeat expansion block nuclear import and export. *Proc Natl Acad Sci U S A*. 2017; 114(7):E1111–E7. <https://doi.org/10.1073/pnas.1620293114> PMID: 28069952

SUPPORTING INFORMATION

Expansion Microscopy Using a Single Anchor Molecule for High-Yield Multiplexed Imaging of Proteins and RNAs

Yi Cui^{1,2¶,#a}, Gaojie Yang^{1,2¶}, Daniel R. Goodwin^{1,2}, Ciara H. O'Flanagan³, Anubhav Sinha^{1,2,4}, Chi Zhang^{1,2}, Kristina E. Kitko^{1,2,#b}, Tay Won Shin^{1,2}, Demian Park^{1,2}, Samuel Aparicio^{3,5}, CRUK IMAXT Grand Challenge Consortium[^], Edward S. Boyden^{1,2,7,8,9,10*}

¹McGovern Institute, Massachusetts Institute of Technology (MIT), Cambridge, MA, USA

²Media Arts & Sciences, MIT, Cambridge, MA, USA

³Department of Molecular Oncology, BC Cancer, Vancouver, BC, Canada

⁴Harvard-MIT Program in Health Sciences and Technology, MIT, Cambridge, MA, USA

⁵Department of Pathology and Laboratory Medicine, University of British Columbia, Vancouver, BC, Canada

⁷Department of Biological Engineering, MIT, Cambridge, MA, USA

⁸Department of Brain and Cognitive Sciences, MIT, Cambridge, MA, USA

⁹Koch Institute for Cancer Research, MIT, Cambridge, MA, USA

¹⁰Howard Hughes Medical Institute, MIT, Cambridge, MA, USA

*Corresponding author: edboyden@mit.edu

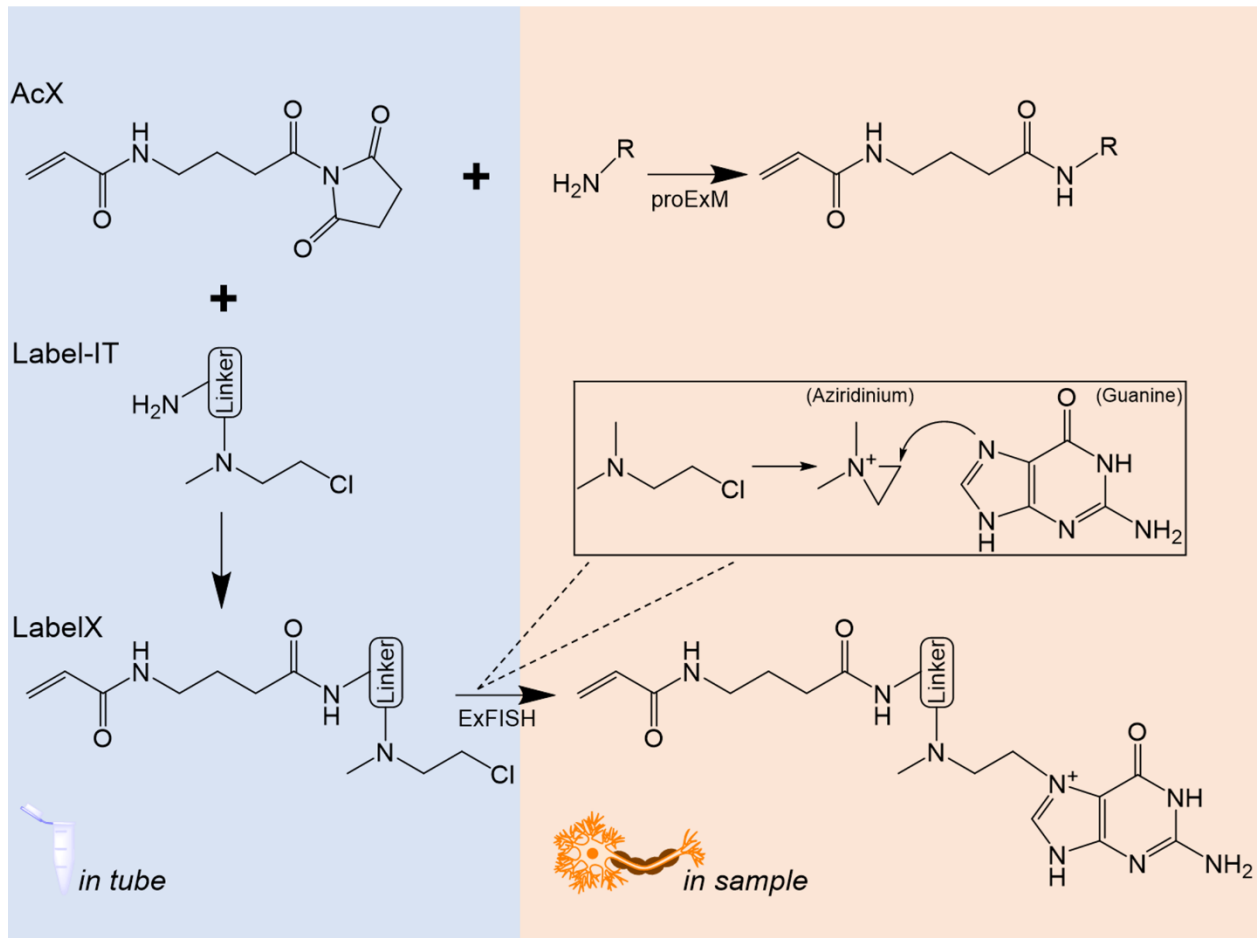
¶These authors contributed equally to this work

#aCurrent address: NanoString Technologies, Inc., Seattle, WA, USA

#bCurrent address: Eli Lilly and Company, San Francisco, CA, USA

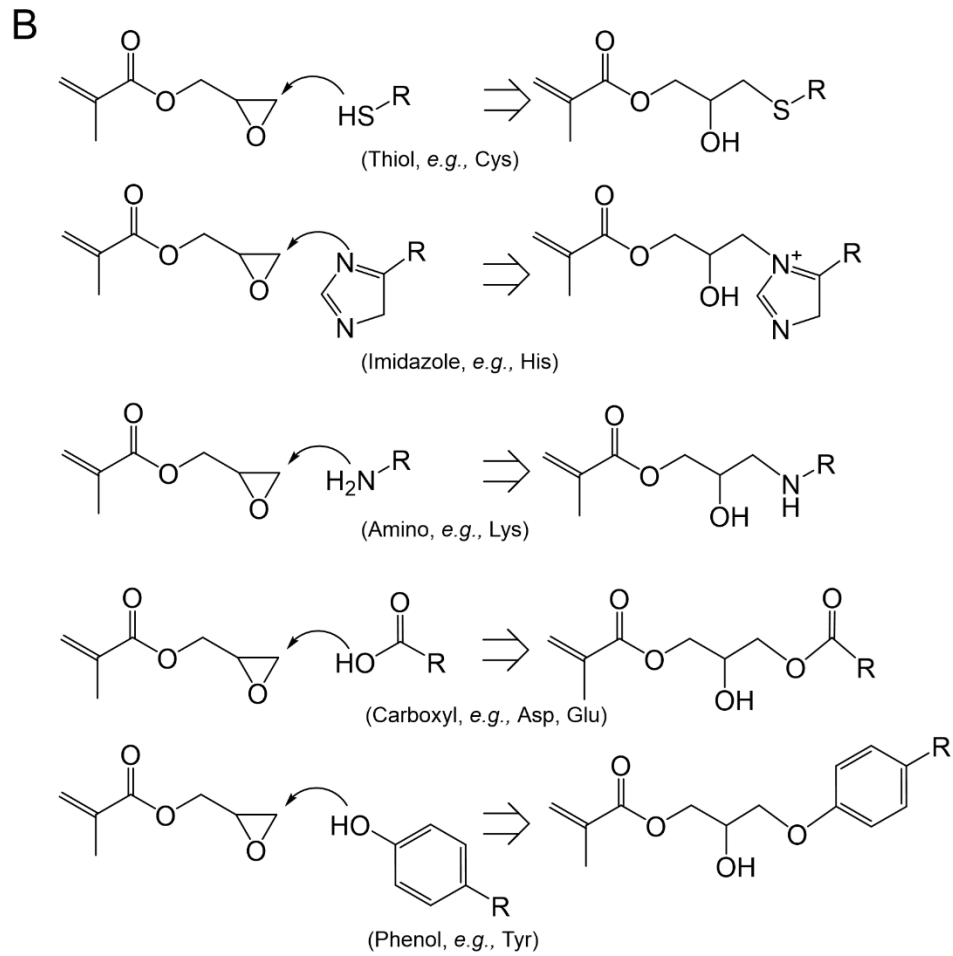
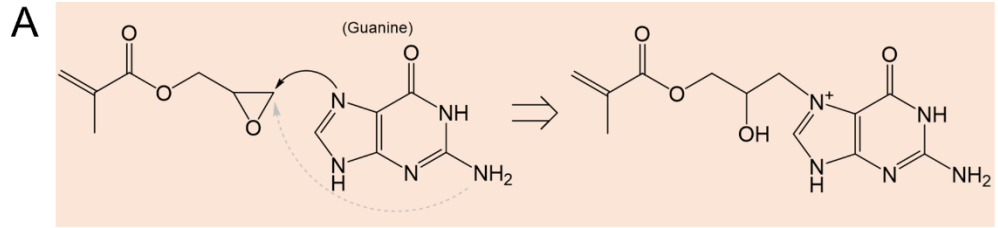
^List of the IMAXT Consortium investigators is provided in the Acknowledgements.

Supplementary Figures

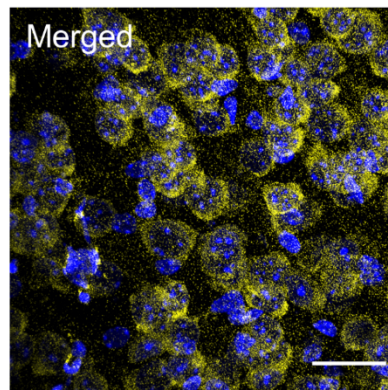
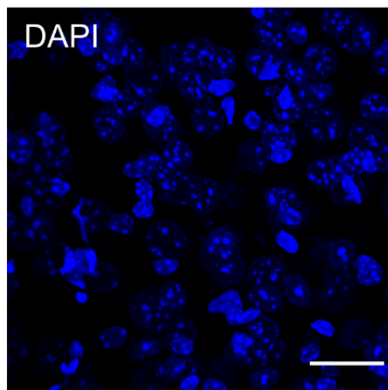
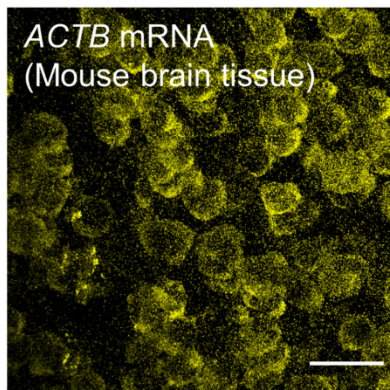
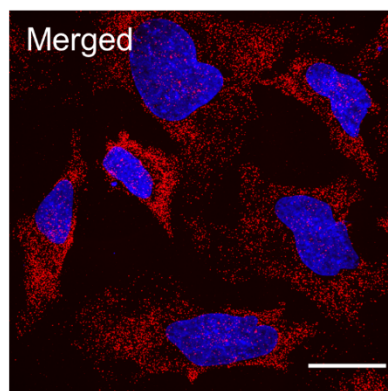
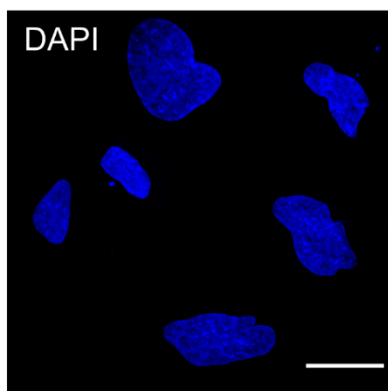
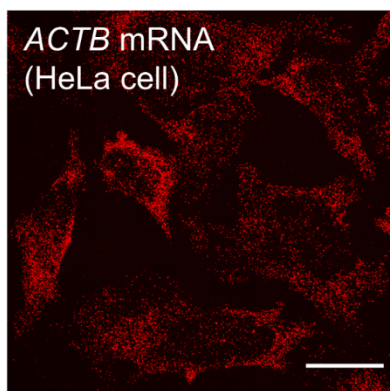
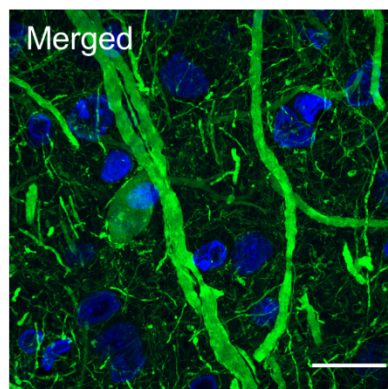
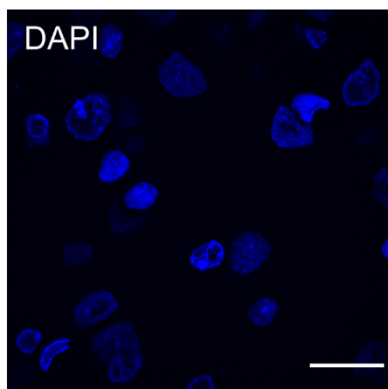
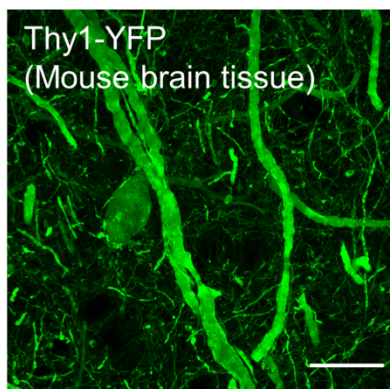
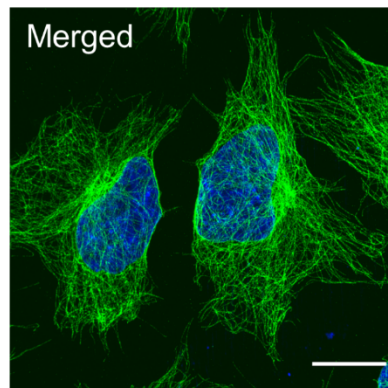
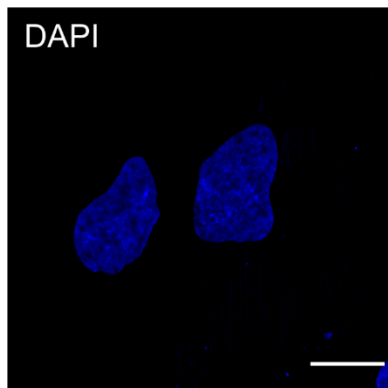
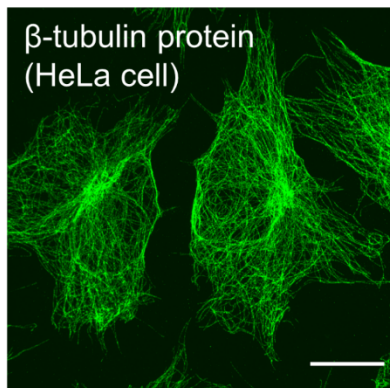


S1 Fig. Working mechanisms of the anchoring chemistry of standard ExM.

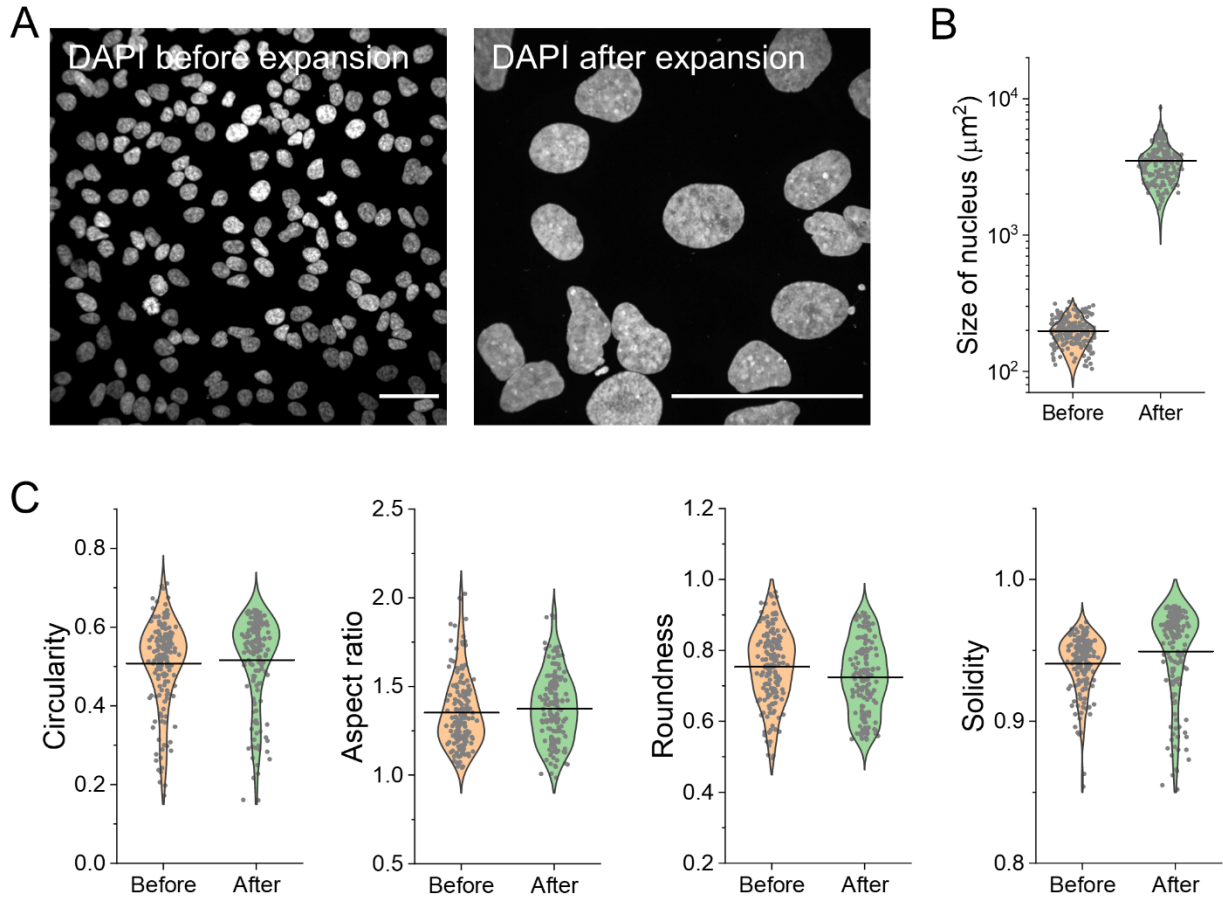
In protein-retention ExM (proExM), AcX functions by modifying the amine groups on proteins through a succinimidyl ester moiety. The acryloyl group of AcX crosslinks the proteins to the polyacrylate hydrogel. In order to anchor nucleic acids, AcX is first reacted with an alkylating reagent such as Label-IT amine to form aziridinium-containing LabelX which can later be coupled to the N7 position of guanine in DNA and RNA. However, this in-house synthesis of anchor molecules suffers from high cost, nonstandard yield, and increased procedure time and complexity.



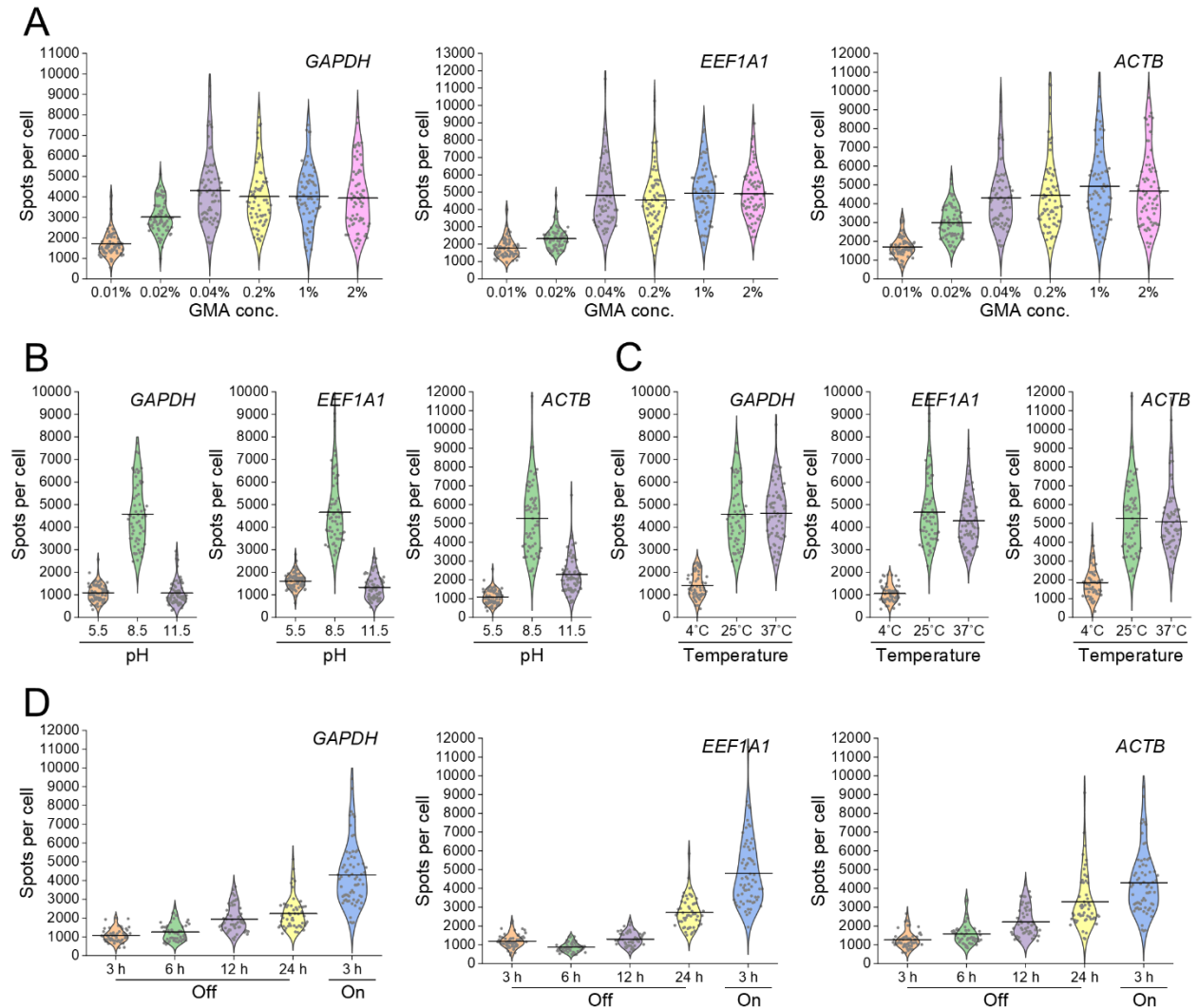
S2 Fig. Representative potential nucleophile substrates in a biological system, including **(A)** nucleic acids and **(B)** amino acids. A potential reaction between GMA and N7-guanine in anchoring DNA and RNA is highlighted in orange. Potential reactions between common nucleophilic amino acids and GMA are illustrated.



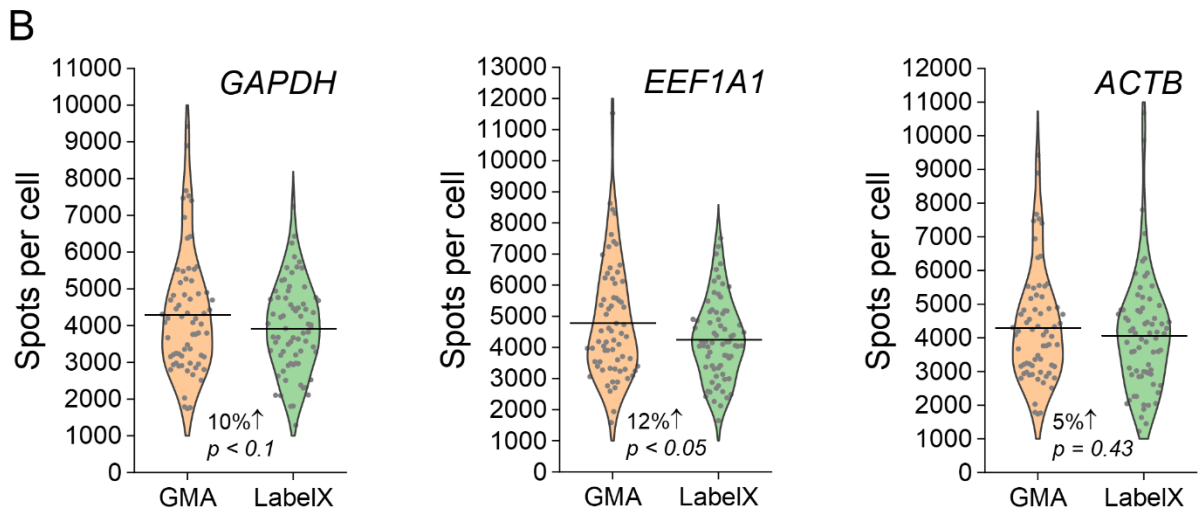
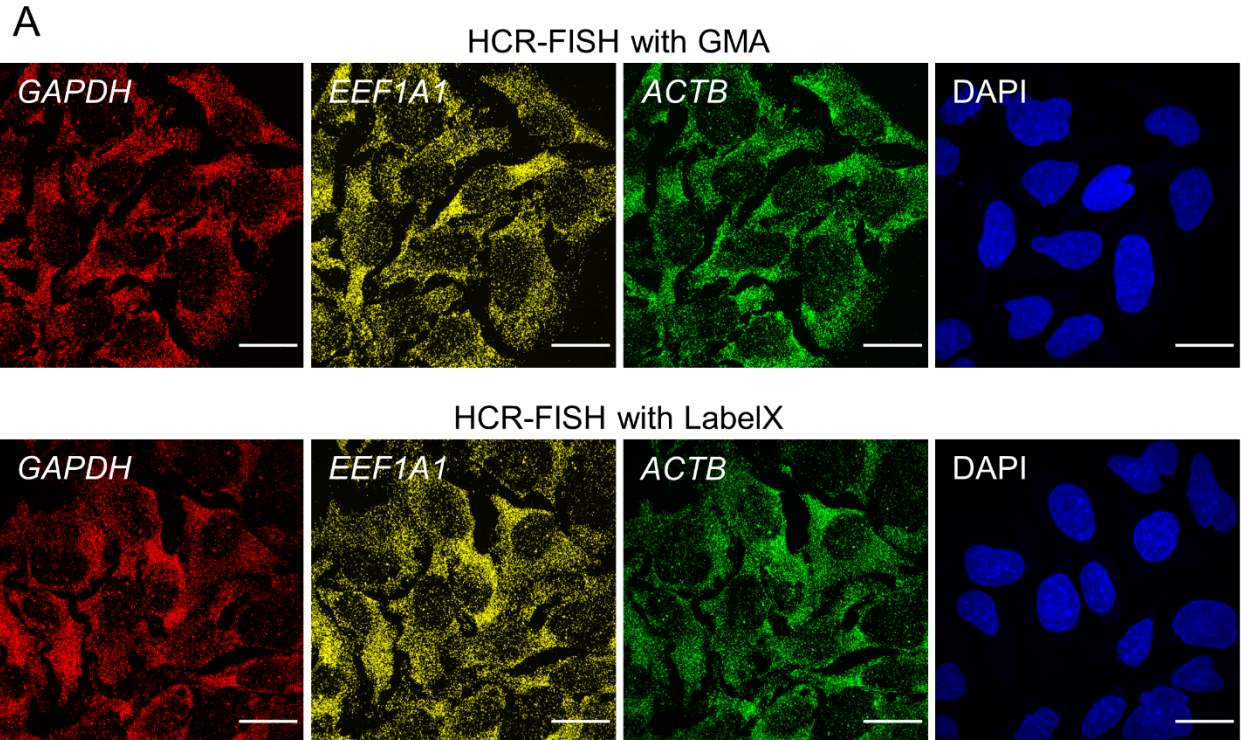
S3 Fig. GMA-based uniExM enables retention of proteins and RNAs in expanded cells and tissues. In protein retention tests, β -tubulin in HeLa cells and YFP in mouse brain tissues were chosen as targets. Row 1: HeLa cells were anchored with 0.04% (w/v) GMA, digested with LysC and stained with anti- β -tubulin (and DAPI) post-expansion. Row 2: A 50 μ m thick Thy1-YFP mouse brain slice was anchored with 0.1% (w/v) GMA, digested with proK, and imaged post-expansion. In RNA retention tests, HCR-FISH targeting *ACTB* in HeLa cells (Row 3) and mouse brain tissues (Row 4) were performed post-expansion, respectively. Color representation in the images: blue – DAPI; green – Thy1-YFP/Alexa488; yellow – Alexa546; red – Alexa647. Scale bars (in pre-expansion units): 20 μ m.



S4 Fig. Assessment of the size and morphological properties of HeLa cell nuclei before and after GMA-based uniExM. (A) Representative images of DAPI staining for HeLa cell nuclei before and after expansion. Scale bars (in pre-expansion units): 50 μm . **(B)** Size of nuclei was measured before and after expansion. **(C)** 4 parameters related to nuclear morphological properties – circularity, aspect ratio, roundness and solidity – were evaluated within ImageJ. (Data presented in violin plots with raw data points shown and mean values highlighted with solid lines, $n = 200$ cells from 4 culture batches, two sample t -test was performed with all $p > 0.1$)



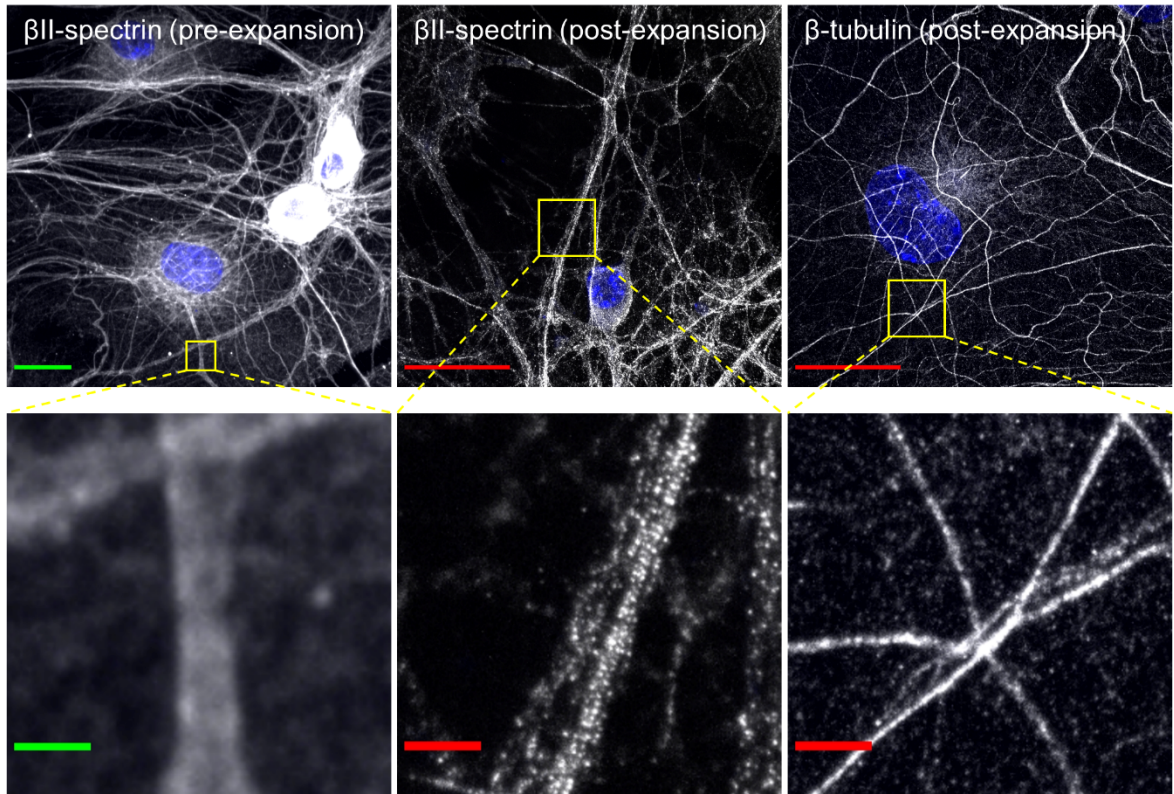
S5 Fig. Optimization for GMA-based RNA anchoring in uniExM. (A) Different concentrations of GMA, **(B)** anchoring pH and **(C)** temperatures were tested in the context of ExFISH targeting three genes – *GAPDH*, *EEF1A1* and *ACTB* – in HeLa cells, to determine optimal RNA retention conditions. **(D)** In light of the above tests, the GMA anchoring reaction for RNAs could be tuned “On” and “Off” by varying the reaction temperature and pH. Reaction “Off” condition: 4°C, pH = 7.4 with 1×PBS. Reaction “On” condition: 25°C, pH = 8.5 with 100 mM NaHCO₃. To test the “Off-On” transition, one group of cells were first incubated under the “Off” condition for 12 h, followed by treatment under the “On” condition for 3 h. (n = 50-80 cells for each tested condition and from 2 culture batches)



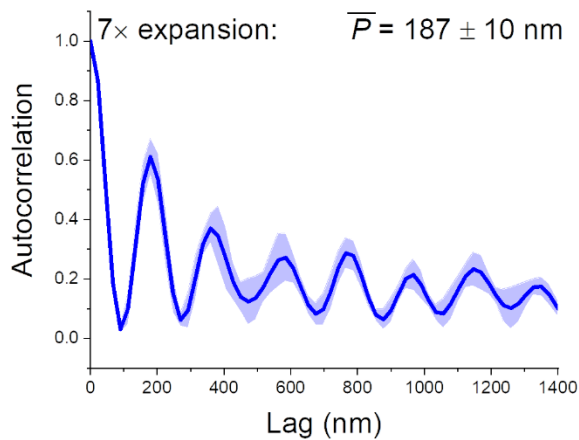
S6 Fig. Head-to-head comparison between GMA and LabelX in RNA retention and detection. (A) HCR-FISH targeting three highly expressed housekeeping genes was performed in HeLa cells treated with 0.04% (w/v) GMA or 0.01% (w/v) LabelX, under their respective optimal conditions. Color representation in the images: blue – DAPI; green – Alexa488; yellow – Alexa546; red – Alexa647. Linear expansion factor: 4.3 for GMA; 4.4 for LabelX (prior to re-embedding). Scale bars (in pre-expansion units): 20 μ m. **(B)** Summary plots of detected transcripts per cell for each gene. (Data presented in violin plots with raw data points shown and mean values highlighted with solid lines; $n = 70-100$)

cells from 3 culture batches; two-sample t -test was performed, with p values shown)

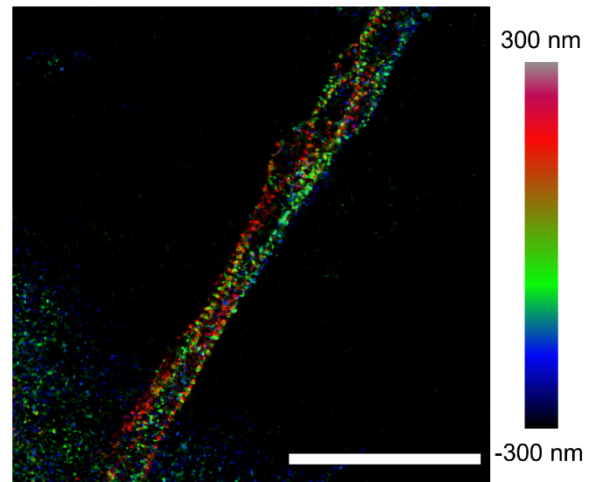
A



B

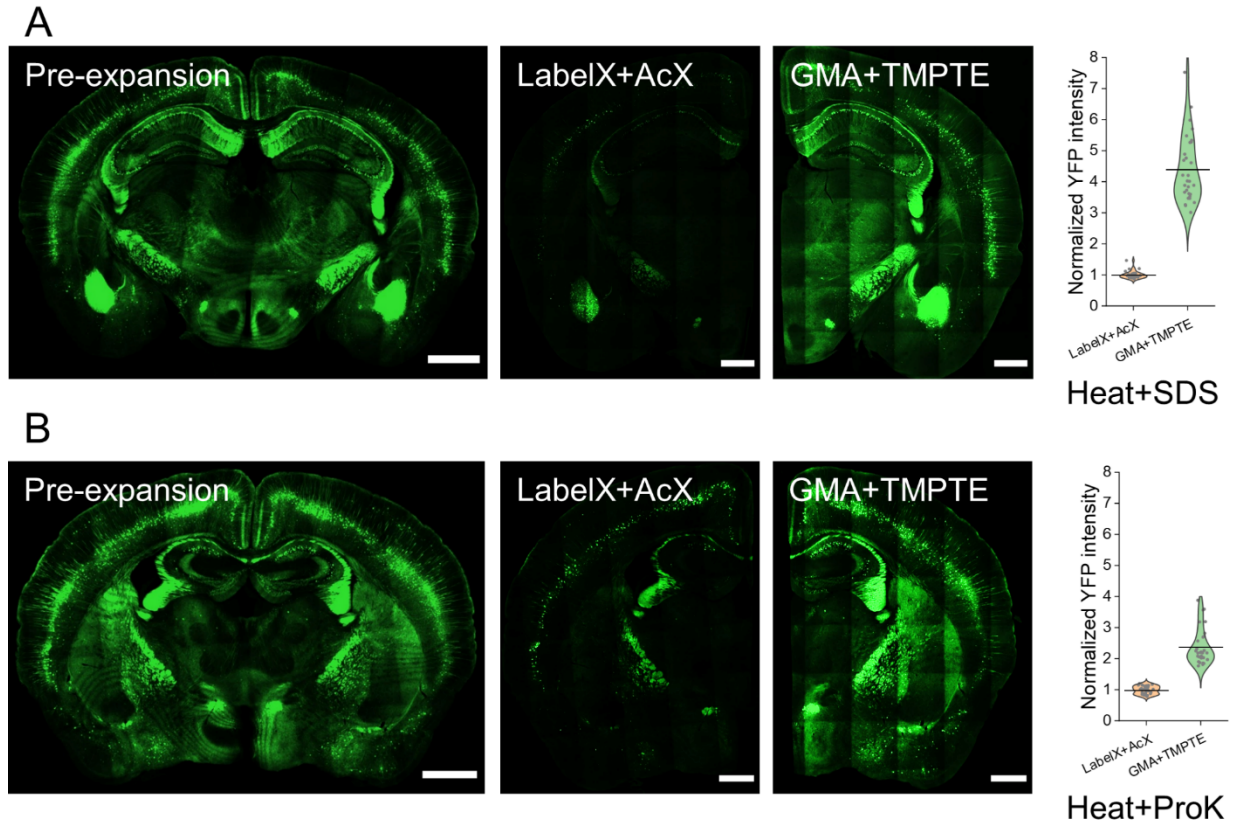


C

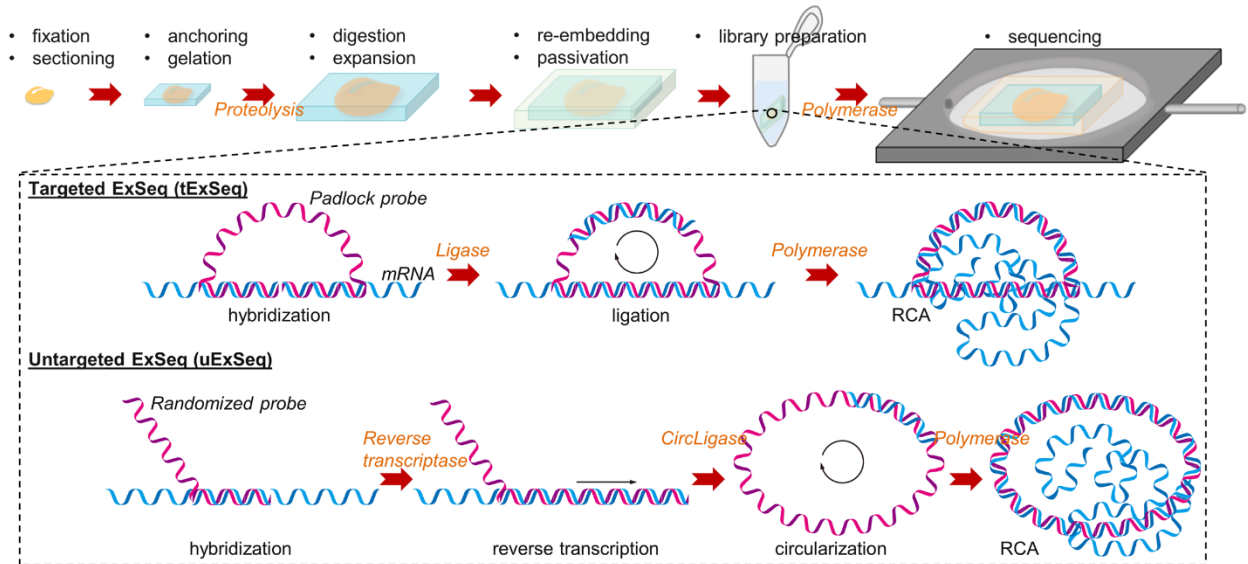


S7 Fig. uniExM helps resolve the ultrastructure of β II-spectrin in neuron axons – additional data. Left column: antibody staining for β II-spectrin in mouse hippocampal neurons shows apparently continuous signal distribution along neuronal processes. Middle column: the periodic, punctate distribution of β II-spectrin signals is revealed, after expansion. Right column: antibody staining against β -tubulin shows continuous microtubule structures even with expansion. All antibody staining was performed pre-expansion. Linear expansion factor: 4.4. Color representation in the images: gray/white – antibody staining; blue – DAPI.

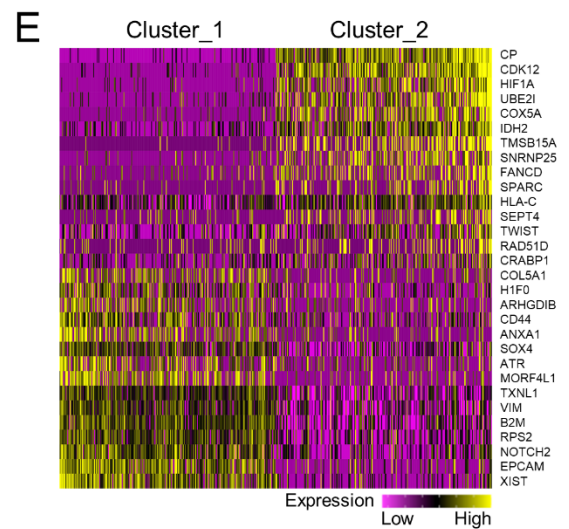
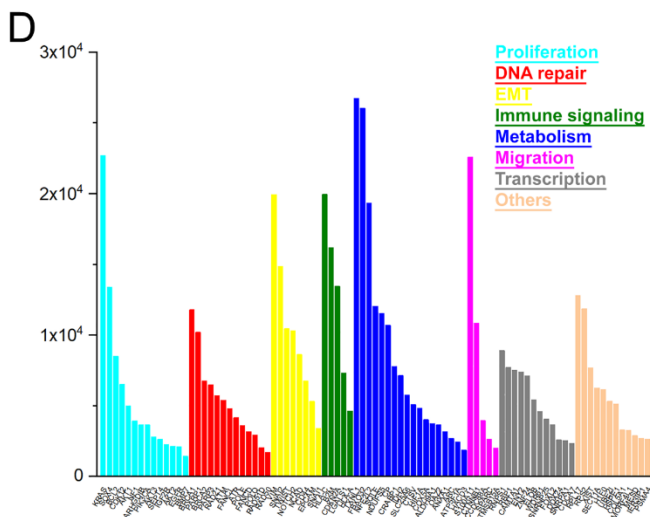
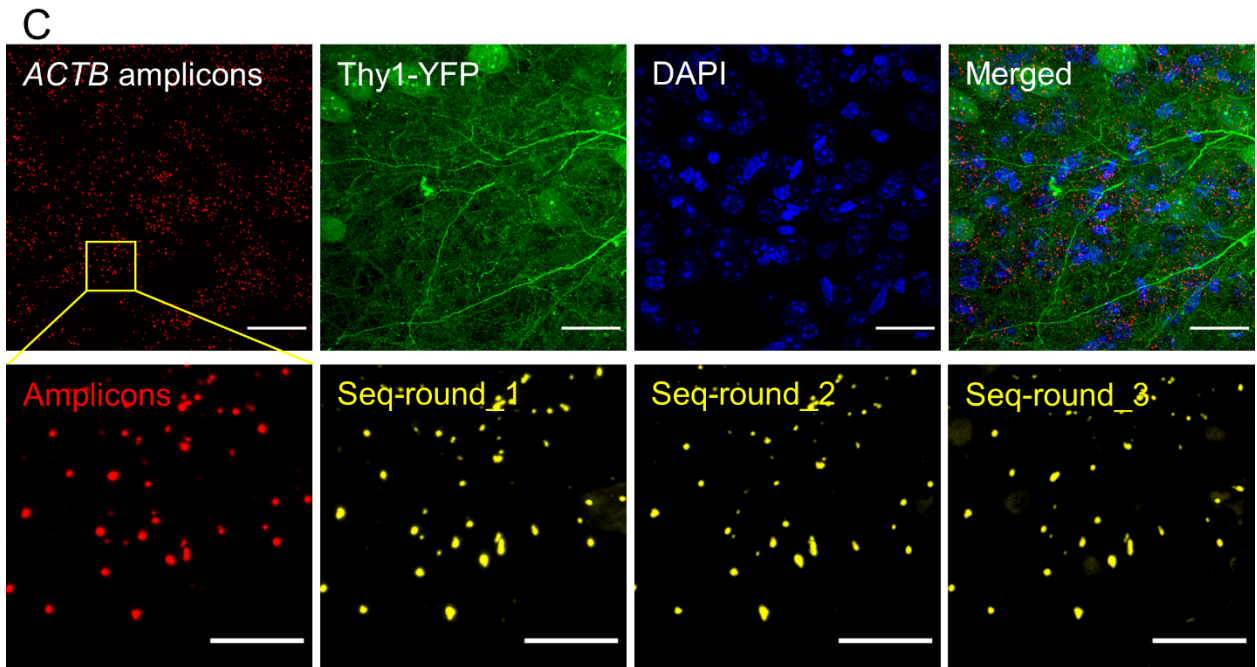
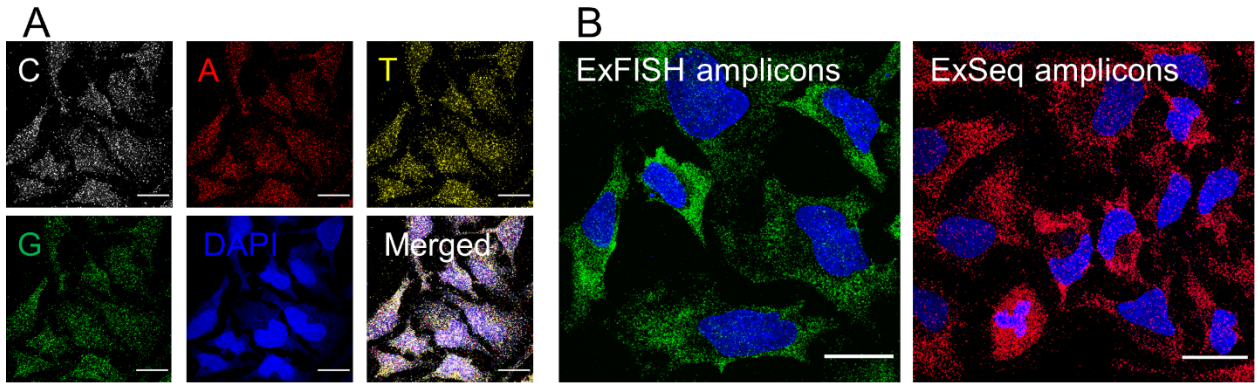
Scale bars (in pre-expansion units): 20 μm (upper panels); 2 μm (lower panels). **(B)** Mean autocorrelation function of periodicity analysis using 7 \times expansion. (Solid lines, mean; shaded areas, standard error of mean. $n = 40$ measurements from 2 culture batches). **(C)** Post-expansion antibody staining revealed the same periodic distribution pattern of βII -spectrin under 7 \times expansion. Scale bar (in pre-expansion units): 5 μm . The color code of the image represents z-axis information.



S8 Fig. Preservation of fluorescent protein function in tissues undergoing high heat treatments by combining acrylate epoxides and polyepoxides. Retention of Thy1-YFP fluorescence signals in mouse brain tissues by LabelX plus AcX vs. GMA plus TMPTE after: (A) strong detergent SDS-based denaturation: 95°C for 1 h, followed by 37°C overnight; (B) ProK-based digestion: 60°C for 2 h, followed by 37°C overnight. Scale bars (in pre-expansion units): 1,000 μm (whole brain); 500 μm (half brain). Normalized YFP intensity measurements are presented in violin plots with mean values highlighted with solid lines. The intensity values were normalized to the level of LabelX plus AcX treated samples. (n = 30 measurements from 4 brain slices, 2 mouse brains; two-sample *t*-test was performed for statistical significance tests, with both $p < 10^{-15}$)



S9 Fig. Schematic illustration for targeted and untargeted ExSeq procedures. After a sample is fixed, sectioned, and expanded, it undergoes a second gelation in a charge-neutral hydrogel (the process of “re-embedding”) followed by neutralization of charge on the original hydrogel (the process of “passivation”) to prepare the sample for sequencing. Then padlock probes targeting specific mRNAs (for tExSeq) or randomized oligonucleotide probes (for uExSeq) are introduced. In tExSeq, the padlock probes are directly ligated upon hybridization to their designated targets, while in uExSeq the randomized probes prime reverse transcription to add sequence information from the bound RNA into cDNA form, followed by probe circularization. The ligated or circularized probes are then subjected to rolling circle amplification (RCA) before being sequenced by ligation or synthesis.



S10 Fig. Demonstration of uniExM for *in situ* RNA sequencing (ExSeq). (A)

Amplicons generated by GMA-based uExSeq in HeLa cells were imaged with SBS reagents (from the Illumina MiSeq v3 kit). The following excitation and emission wavelengths were used for 5-channel acquisition: DAPI – Ex. 405 nm / Em. 440-460 nm; Base “G” – Ex. 488 nm / Em. 500-550 nm; Base “T” – Ex. 561 nm / Em. 575-590 nm; Base “A” – Ex. 640 nm / Em. 663-737 nm; Base “C” – Ex. 685 nm / Em. 705-845 nm. Scale bars (in pre-expansion units): 20 μm .

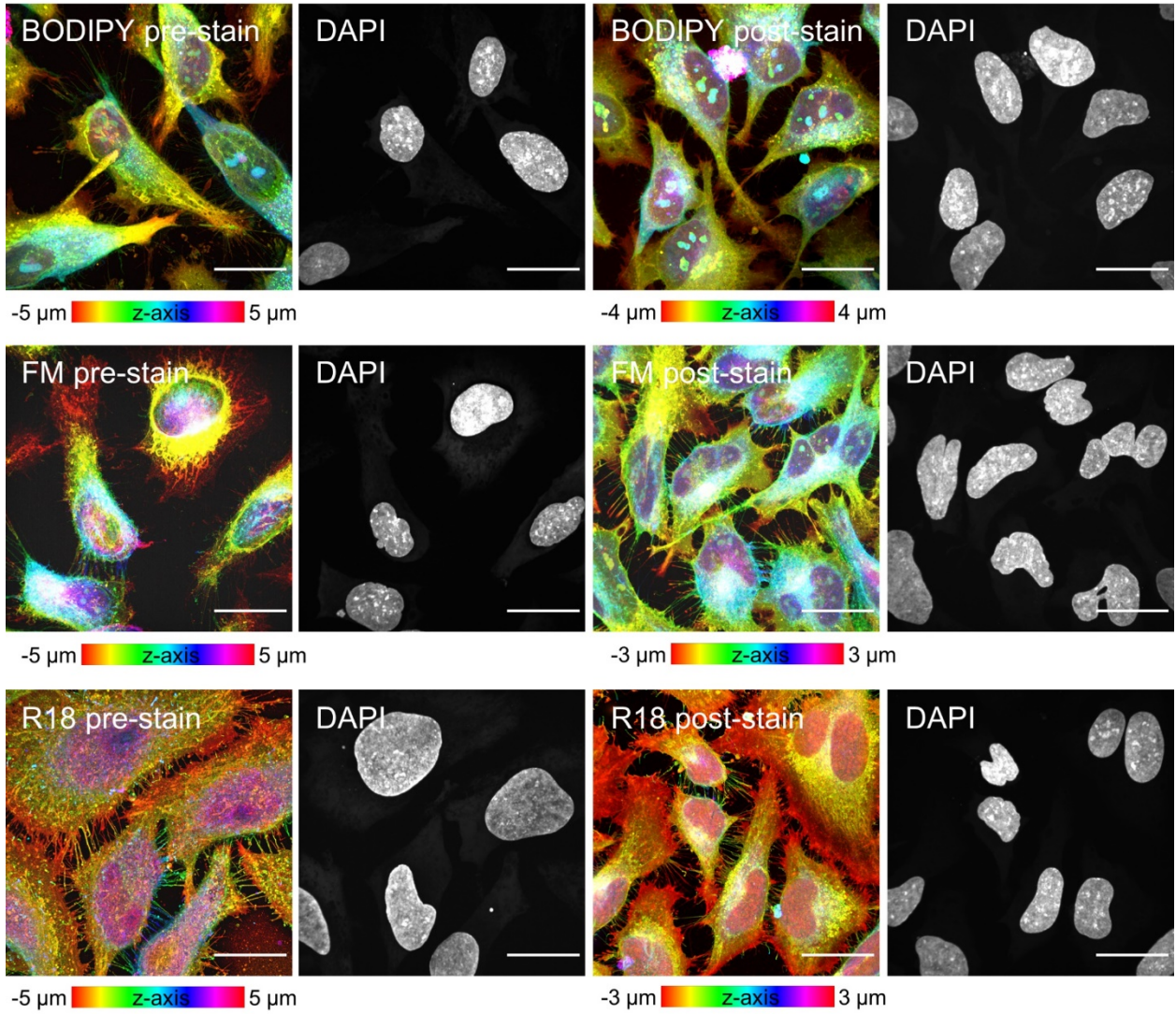
(B) Characterization of uniExM for *in situ* enzymatic amplification in tExSeq. *GAPDH* mRNAs were amplified by HCR-FISH (ExFISH) or padlock probes in tExSeq. Then the generated signal spots in individual cells were counted. For better comparison, Alexa546 conjugated oligonucleotide probes were used for amplicon detection in both cases. Scale bars (in pre-expansion units): 20 μm .

(C) Characterization of uniExM for *in situ* enzymatic sequencing in tExSeq. tExSeq targeting *ACTB* mRNAs in Thy1-YFP mouse brain tissues was performed, where padlock probes bearing consecutive bases “TTT” as the barcode were used. Before *in situ* sequencing, imaging with universal amplicon detection probes was performed to establish a reference image for the transcript locations (lower left, red). YFP signals were also imaged. After that, the universal probes and YFP signals were removed by concentrated formamide and heat treatment. Next, three rounds of SBS were conducted and the detected signal spots were benchmarked against the reference amplicon image (lower row, yellow dots). Scale bars (in pre-expansion units): 20 μm (for upper panel), 5 μm (for lower panel).

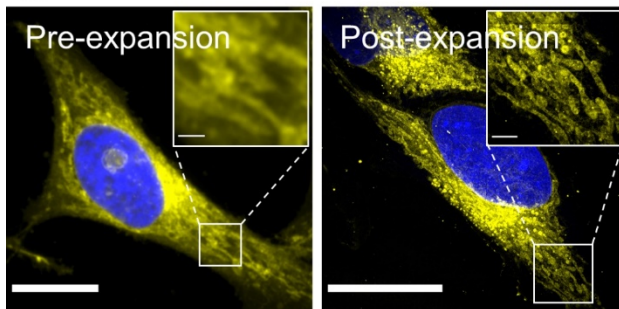
(D) tExSeq targeting 87 cancer clone-specific genes in SA501 PDX breast cancer tissue was performed using 7-round SBS. All the decoded transcripts from a $\sim 0.8 \text{ mm}^2$ tissue slice, along with their function annotations, are summarized in the bar chart.

(E) Principal component analysis (PCA) identified two groups of genes (15 each) that classify the tissue cells into two primary groups.

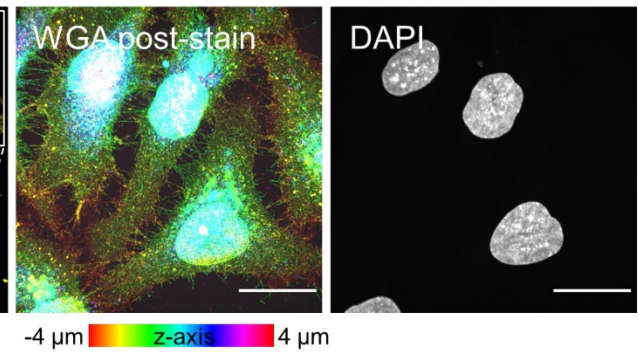
A



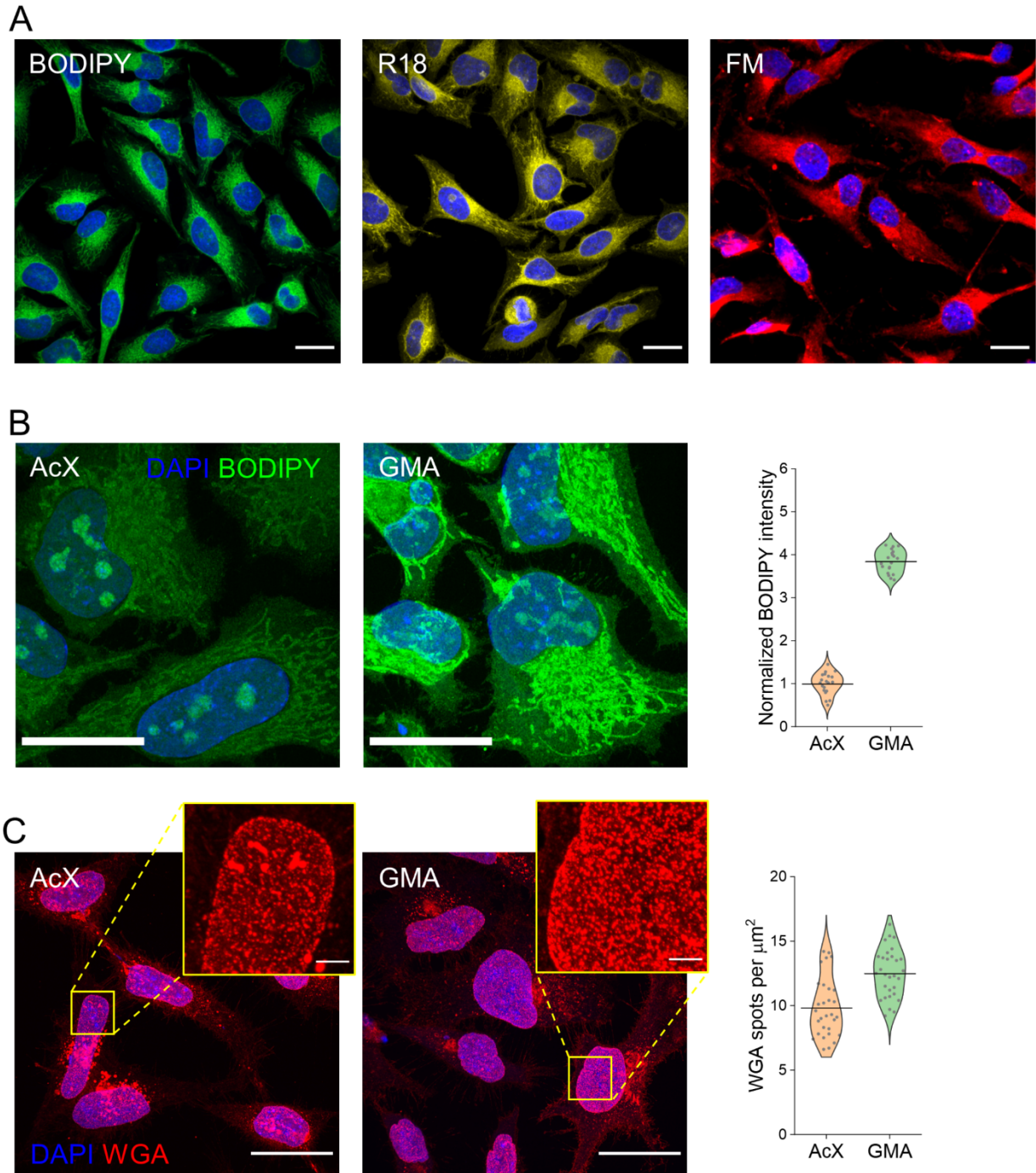
B



C



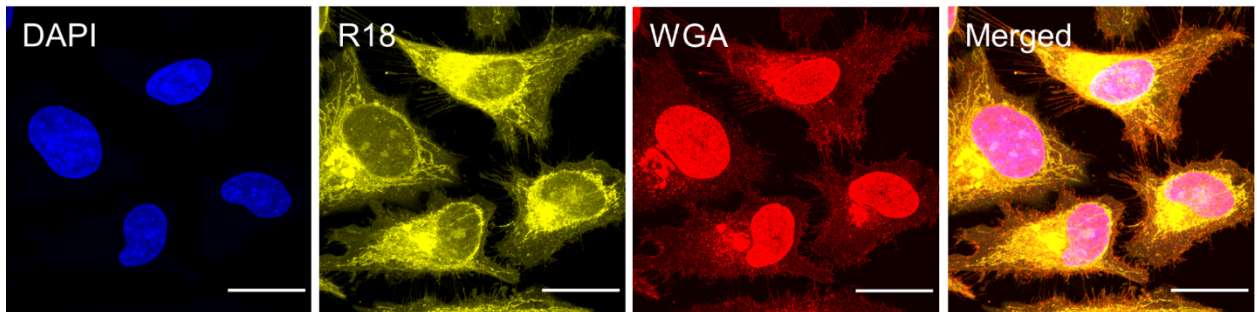
S11 Fig. Qualitative demonstration of detection of lipids and carbohydrates in uniExM. (A) Commercially available lipid staining reagents – BODIPY, FM and R18 – were tested in HeLa cells in the context of both pre- and post-expansion staining. As shown here, all three staining reagents exhibit consistent image patterns in pre- and post-expansion staining. The color-code in the lipid signal channel represents z-axis information. Scale bars (in pre-expansion units): 20 μm . **(B)** Detection of lipids expands the biological information that can be obtained by uniExM. In the expanded sample, post-expansion staining with lipophilic fluorophore R18 helps better resolve lipid-rich mitochondria where cristae are only discernible with expansion (highlighted in the zoomed-in inset). Scale bars (in pre-expansion units): 20 μm (large images); 1 μm (insets). **(C)** WGA-A647 was used to stain carbohydrates/glycoconjugates post-expansion in HeLa cells digested with the selective protease LysC. Strong signals were detected on cell and nuclear membranes. Color in the WGA channel represents z-axis information. Scale bars (in pre-expansion units): 20 μm .



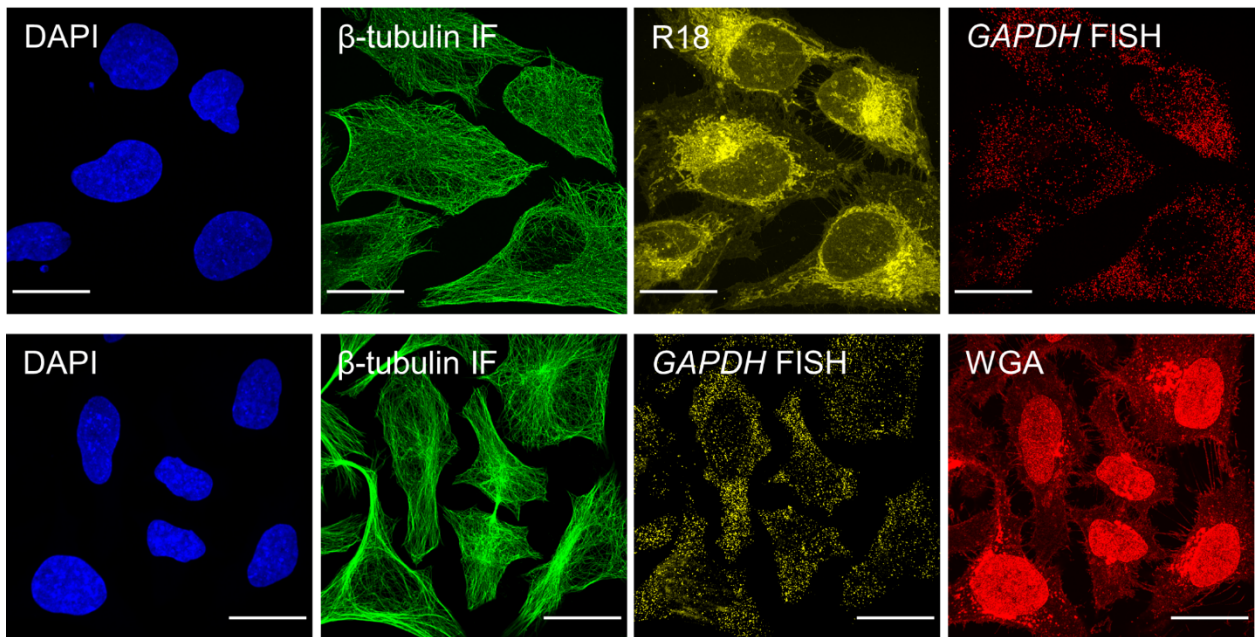
S12 Fig. Qualitative and partial quantitative detection of lipids and glycoproteins (*i.e.*, carbohydrates) in HeLa cells treated with different anchors. (A) Normal staining patterns for the three selected lipid tags in 4% PFA fixed HeLa cells. Scale bars: 20 μm . (B) Comparison between AcX and GMA treatments in visualizing lipid structures. HeLa cells were treated with 0.01% (w/v) AcX or 0.04% (w/v) GMA, followed by expansion and staining with DAPI and BODIPY. Fluorescence intensity measurements are presented in violin plots

with mean values highlighted with solid lines. The intensity values were normalized to the level of AcX treated samples. (n = 20 images from 2 culture batches; two-sample *t*-test was performed for statistical significance, with $p < 10^{-10}$). Scale bars (in pre-expansion units): 20 μm . **(C)** Comparison between AcX and GMA treatments in visualizing glycoprotein-enriched putative nucleoporins on nuclear membranes. Post-expansion staining with WGA in HeLa cells treated with GMA showed potentially better molecular retention, which in turn yielded a larger number of putative nucleoporin puncta, as compared to those of AcX treated samples. Scale bars (in pre-expansion units): 20 μm (zoomed-out images); 2 μm (zoomed-in images). WGA signal spots per μm^2 were quantified (n = 30 cells from 2 culture batches; two-sample *t*-test was performed for statistical significance tests, with $p < 10^{-5}$).

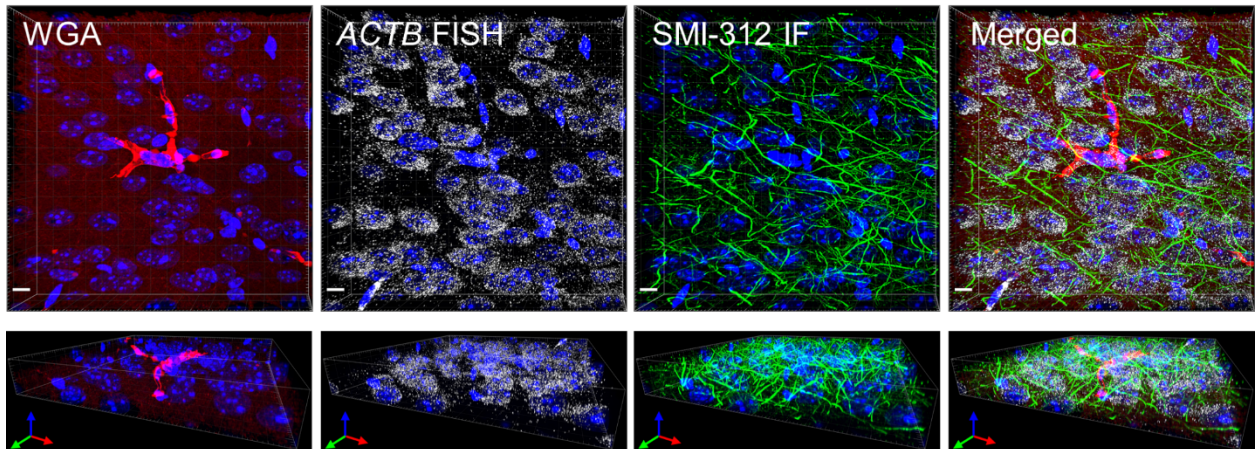
A



B

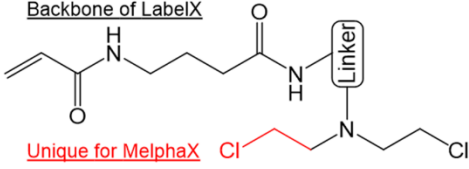
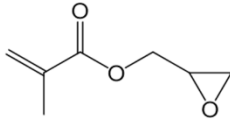
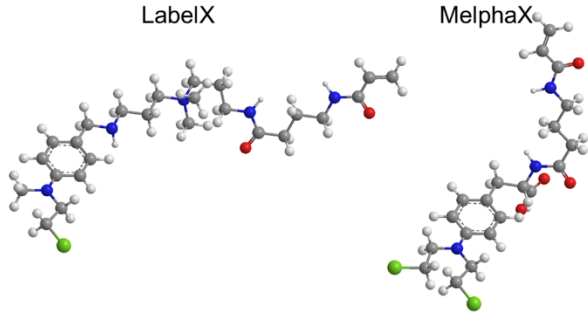
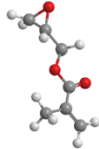
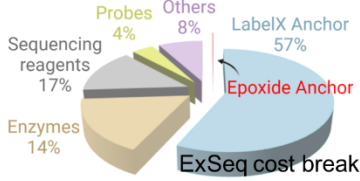


C



S13 Fig. Qualitative demonstration of uniExM imaging of multiple biomolecular species. (A) Demonstration of post-expansion co-staining for carbohydrates and lipids. HeLa cells were processed with 0.04% (w/v) GMA and LysC proteolysis, followed by staining with 10 µg/mL R18 and 5 µg/mL WGA-A647. Linear expansion factor: 4.3. Scale bars (in pre-expansion units): 20 µm. **(B)** Lipid or carbohydrate staining can be combined with protein and RNA detection in the same sample. As demonstrated in this figure, β-tubulin was stained with antibody pre-expansion, while R18, WGA staining and HCR-FISH were performed post-expansion. In addition to target-specific detection by IF (immunofluorescence) and FISH, staining for lipids and carbohydrates provides structural information at the cellular (*e.g.*, membranes) or subcellular levels (*e.g.*, mitochondria). Scale bars (in pre-expansion units): 20 µm. **(C)** Demonstration of multimodal detection by uniExM at the tissue level. In a 50 µm mouse brain tissue, HCR-FISH targeting *ACTB*, IF using SMI-312 antibody (against neurofilament) and WGA stain (contrast adjusted to highlight blood vessels) were applied together. Image stacks were rendered in 3D and presented in the lower panel. The colors in images correspond to the following fluorescent dyes: blue – DAPI; green – Alexa488; gray – Alexa546; red – Alexa647. Scale bars (in pre-expansion units): 5 µm.

Supplementary Tables

	In-house synthesized RNA anchor: LabelX, MelphaX	Acrylate epoxide multifunctional anchor: GMA
Chemical formula	 <p>Backbone of LabelX</p> <p>Unique for MelphaX</p>	
3D structure	 <p>LabelX</p> <p>MelphaX</p>	 <p>GMA</p>
Molecular weight	LabelX: ~520 MelphaX: ~440	~140
Reactive moiety	Aziridinium	Epoxide
Primary anchoring substrates	Nucleic acids (via Guanine-N7)	Major intracellular nucleophiles, including nucleic acids, proteins and other biomolecules
Anchoring time	>10 h (at 37°C, pH 7.7)	3 h (at RT or 37°C, pH 8.5)
Working conc.	LabelX: 0.01% (w/v) for tissue MelphaX: 0.1% (w/v) for tissue	0.04% (w/v) for cultured cell 0.1% (w/v) for tissue
Stability	~6 months at -20°C	>2 years at 2-8°C
Cost per unit*	LabelX: ~\$7,500/mg MelphaX: ~\$70/mg	\$0.0003/mg
Cost per sample (e.g., 50 µm thick mouse brain slice)	LabelX: ~\$180 MelphaX: ~\$40	~\$0.000075
Total cost for one multiplexed expt. on a 1 cm ² tissue (e.g., PDX slice)	LabelX: ~\$200 (2-plex proExM+ExFISH) ~\$210 (4-plex ExFISH) ~\$300 (100-plex ExSeq) MelphaX: ~\$60 (2-plex proExM+ExFISH) ~\$70 (4-plex ExFISH) *Not tested in 100-plex ExSeq	~\$20 (2-plex proExM+ExFISH) ~\$30 (4-plex ExFISH) ~\$120 (100-plex ExSeq)  <p>ExSeq cost breakdown</p>

S1 Table. High-level comparison of LabelX, MelphaX and GMA for key parameters in multimodal ExM applications

Antibody name	Vendor information	Catalog number
Mouse anti-tubulin	DSHB	E7
Rabbit anti-GFP	ThermoFisher Scientific	A-6455
Mouse anti- β II-spectrin	BD Biosciences	612563
Mouse anti-MAP2	BioLegend	801801
Mouse anti-SMI312	BioLegend	837904
Goat anti-mouse IgG Alexa 488	ThermoFisher Scientific	A-21430
Goat anti-rabbit IgG Alexa 555	ThermoFisher Scientific	A-11017
Goat anti-mouse IgG Alexa 546	ThermoFisher Scientific	A-11018
Goat anti-rabbit IgG Alexa 647	ThermoFisher Scientific	A-21246

S2 Table. Main antibodies used in this study

Chemical/Reagent Name	Supplier	Catalog #
16% Formaldehyde (w/v), methanol-free (PFA)	Thermo Fisher	28908
4',6-diamidino-2-phenylindole (DAPI)	Sigma	D9542
4-Hydroxy-TEMPO (4-HT)	Sigma	176141
Acrylamide (AA)	Sigma	A9099
Acrylamide/Bis 19:1, 40% (w/v) solution	Thermo Fisher	AM9022
Acryloyl-X, SE, 6-((acryloyl)amino)hexanoic Acid, Succinimidyl Ester (AcX)	Thermo Fisher	A20770
Aminoallyl-dUTP solution (50 mM)	Thermo Fisher	R1101
Ammonium persulfate (APS)	Sigma	A3678
Bind-silane	Sigma	GE17-1330-01
BODIPY FL C ₁₂	Thermo Fisher	D3822
CircLigase II ssDNA ligase	Lucigen	CL9025K
Deoxynucleotide (dNTP), 10 mM solution mix	NEB	N0447L
Dideoxynucleoside triphosphate set (ddNTP)	Roche	03732738001
DMEM	Thermo Fisher	10569010
DMSO, Anhydrous	Thermo Fisher	D12345
DTT	Roche	37016821
DPBS, 1×	Corning	21-031-CV
EDTA, 0.5M solution, pH 8.0	Thermo Fisher	15575020
Endonuclease V	NEB	M0305S

Endoproteinase LysC	NEB	P8109S
Ethanolamine hydrochloride	Sigma	E6133
Fetal bovine serum	Thermo Fisher	16000036
FM 1-43 FX membrane stain	Thermo Fisher	F35355
Formamide (deionized)	Thermo Fisher	AM9344
Glutaraldehyde (GA), 25% solution	Sigma	G5882
Glycidyl methylacrylate (GMA)	Sigma	151238
Guanidine hydrochloride	Sigma	50937
HCR-FISH probes, amplifiers and buffers	Molecular Instruments	N/A
Inosine	Sigma	I4125
Label-IT amine	Mirus Bio	MIR3900
MAXpack immunostaining media kit	Active Motif	15251
MES, 0.5M solution, pH 6.5	Alfa Aesar	J63778
MiSeq reagent kit v3	Illumina	MS-102-3003
N-(3-Dimethylaminopropyl)-N'-ethylcarbodiimide hydrochloride (EDC)	Sigma	03450
N,N,N',N'-Tetramethylethylenediamine (TEMED)	Sigma	T7024
N,N'-Methylenebisacrylamide (BIS)	Sigma	M7279
N-Hydroxysuccinimide (NHS)	Thermo Fisher	24500
Octadecyl rhodamine B chloride (R18)	Thermo Fisher	O246
PBCV-1 DNA ligase	NEB	M0375L
PBS, 10×	Thermo Fisher	70011044
PEGylated bis(sulfosuccinimidyl)suberate (BE(PEG)9)	Thermo Fisher	21582
Penicillin-streptomycin (10,000 U/mL)	Thermo Fisher	15140122
phi29 DNA polymerase	Enzymatics	P7020-HC-L
Proteinase K	NEB	P8107S
RNase A	Thermo Fisher	EN0531
RNase H	NEB	M0297L
RNase inhibitor	NEB	M0314S
Sigmacote	Sigma	SL2
Sodium acrylate (SA)	Sigma	408220
Sodium bicarbonate, powder	Sigma	S6014
Sodium borate, 0.5M solution, pH 8.5	Alfa Aesar	J62902
Sodium borohydride	Sigma	213462
Sodium chloride, 5M solution	Sigma	59222C
Sodium dodecyl sulfate (SDS), 20% solution	Sigma	05030
SSC buffer, 20×	Promega	V4261
Standard Taq reaction buffer (with magnesium chloride)	NEB	B9014S
SuperScript IV reverse transcriptase	Thermo Fisher	18090050
Terminal transferase	NEB	M0315L
TetraSpeck microspheres, 0.5 μm	Thermo Fisher	T7281
Trimethylolpropane triglycidyl ether (TMPTE)	Sigma	430269
Tris buffer, 1M solution, pH 8.0, RNase-free	Thermo Fisher	AM9856
Triton X-100	Sigma	T8787

Trypsin-EDTA (0.25% with phenol red)	Thermo Fisher	25200072
Tween 20	Sigma	P9416
UltraPure DNase/RNase-free distilled water	Thermo Fisher	10977023
Wheat germ agglutinin (WGA)-Alexa Fluor 647	Thermo Fisher	W32466
Zwittergent 3-10 detergent	Sigma	693021

S3 Table. Main chemicals and reagents used in this study

Figure	Sample type	Anchoring condition	Detection module
Fig. 1B (i-ii)	Mouse brain slices	0.1% GMA, 100 mM NaHCO ₃ (pH 8.5), 3-6 h pre-incubation at 4°C and 3 h at 37°C	post-expansion HCR-FISH + YFP signal analysis
Fig. 1B (iii)	Human HeLa cells; Mouse hippocampal neurons	0.04% GMA, 100 mM NaHCO ₃ (pH 8.5), 3 h at 37°C	pre-expansion IF + post-expansion HCR-FISH
Fig. 2A	Human HeLa cells	0.04% GMA, 100 mM NaHCO ₃ (pH 8.5), 3 h at RT	pre-expansion IF
Fig. 2B	Human HeLa cells	0.04% GMA, 100 mM NaHCO ₃ (pH 8.5), 3 h at RT	pre-expansion HCR-FISH + post-expansion HCR-FISH
Fig. 3	Mouse hippocampal neurons	0.04% GMA, 100 mM NaHCO ₃ (pH 8.5), 3 h at 37°C	pre- or post-expansion IF
Fig. 4B (ii) Fig. S10A	Human HeLa cells	0.04% GMA, 100 mM NaHCO ₃ (pH 8.5), 6 h at RT	untargeted in situ sequencing
Fig. 4C	Human PDX breast cancer tissues	0.1% GMA, 6 h at 4°C (with 1× PBS, pH 7.4) plus overnight at RT (with 100 mM NaHCO ₃ , pH 8.5)	targeted in situ sequencing
Fig. S3	Human HeLa cells; Mouse brain slices	0.04% GMA, 100 mM NaHCO ₃ (pH 8.5), 3 h at RT; 0.1% GMA, 100 mM NaHCO ₃ (pH 8.5), 3-6 h pre-incubation at 4°C and 3 h at 37°C (for mouse brain)	post-expansion IF or post-expansion HCR-FISH
Fig. S4	Human HeLa cells	0.04% GMA, 100 mM NaHCO ₃ (pH 8.5), 3 h at RT	DAPI staining before imaging
Fig. S5	Human HeLa cells	as indicated in plots	post-expansion HCR-FISH
Fig. S6	Human HeLa cells	0.04% GMA, 100 mM NaHCO ₃ (pH 8.5), 3 h at RT	post-expansion HCR-FISH
Fig. S7	Mouse hippocampal neurons	0.04% GMA, 100 mM NaHCO ₃ (pH 8.5), 3 h at 37°C	pre- or post-expansion IF
Fig. S8	Mouse brain slices	0.05% GMA + 0.05% TMPTE, 6 h at 4°C (with 1× PBS, pH 7.4) plus overnight at RT (with 100 mM NaHCO ₃ , pH 8.5)	post-expansion YFP signal analysis
Fig. S10C	Mouse brain slices	0.1% GMA, 6 h at 4°C (with 1× PBS, pH 7.4) plus overnight at RT (with 100 mM NaHCO ₃ , pH 8.5)	targeted in situ sequencing
Fig. S11A-B Fig. S12B	Human HeLa cells	0.04% GMA, overnight at 4°C (with 1× PBS, pH 7.4) plus 3 h at RT (with 100 mM NaHCO ₃ , pH 8.5)	pre-expansion or post-expansion lipid tag staining
Fig. S11C Fig. S12C	Human HeLa cells	0.04% GMA, 100 mM NaHCO ₃ (pH 8.5), 3 h at RT	post-expansion WGA staining
Fig. S13A	Human HeLa cells	0.04% GMA, overnight at 4°C (with 1× PBS, pH 7.4) plus 3 h at RT (with 100 mM NaHCO ₃ , pH 8.5)	post-expansion R18 + WGA staining
Fig. S13B	Human HeLa cells	0.04% GMA, overnight at 4°C (with 1× PBS, pH 7.4) plus 3 h at RT (with 100 mM NaHCO ₃ , pH 8.5)	pre-expansion IF + post-expansion HCR-FISH + post-expansion R18 or WGA staining

Fig. S13C	Mouse brain slices	0.1% GMA, overnight at 4°C (with 1× PBS, pH 7.4) plus 3 h at RT (with 100 mM NaHCO ₃ , pH 8.5)	pre-expansion IF + post-expansion HCR-FISH + post-expansion WGA staining
-----------	--------------------	--	--

S4 Table. Anchoring conditions used in main experiments

Gene function annotation

Proliferation	DNA repair	EMT	Immune signaling	Metabolism	Migration	Transcription	Others
KRAS	BRCA1	VIM	HLA-C	TXNL1	S100A11	RNPS1	RPL17
SOX4	PARP1	SNAI2	B2M	FBXO32	CTNNB1	RBP1	RPS2
BCL2	BRCA2	TWIST	CDKN2A	NFE2L2	CCDC88A	CAMTA1	XIST
CDK12	PARP3	NOTCH2	LGALS1	SQLE	SPARC	ENY2	SEC11A
AKT1	RAD21	NCAD	HLA-A	NDUFS5	TMSB15A	ZNF24	H1FO
NF1	ATM	CD44		CP		ELOB	UBE2I
ARHGDIB	FANCL	EPCAM		CRABP1		WDR61	HSPE1
PIK3CA	ATR	SNAI1		IDH2		SNRNP25	COL5A1
AKT3	POLE			SLC25A6		FOXL2	MORF4L1
SEPT4	FANCD			CTSV		DDX24	MESD
IGF2R	POLQ			HIF1A		SNRPA1	IER3IP1
AKT2	RAD51D			COX5A		CDCA7	PSMA4
EGFR	RAD50			ALDH9A1			
BMP7				OAZ2			
				ANXA1			
				ARC			
				ATP5F1A			
				HACD3			

S5 Table. Gene list used for profiling SA501 PDX cancer tissues